

Novel Channel Estimation Methods for GFDM Systems in High Mobility Scenario

Hamidreza Shayanfar

A Thesis

in the Department of

Electrical and Computer Engineering

Presented in Partial Fulfillment of the Requirements

for the Degree of

Master of Applied Science at

Concordia University

Montréal, Québec, Canada

March 2025

© Hamidreza Shayanfar, 2025

CONCORDIA UNIVERSITY

School of Graduate Studies

This is to certify that the thesis prepared

By: **Hamidreza Shayanfar**

Entitled: **Novel Channel Estimation Methods for GFDM Systems in High Mobility Scenario**

and submitted in partial fulfillment of the requirements for the degree of

Master of Applied Science

complies with the regulations of this University and meets the accepted standards with respect to originality and quality.

Signed by the Final Examining Committee:

Dr. M. Omair Ahmad Chair and Examiner

Dr. Jun Cai Examiner

Dr. Wei-Ping Zhu Supervisor

Dr. M.N.S. Swamy Co-Supervisor

Approved by _____
Dr. Jun Cai, Graduate Program Director

_____ 2025

Dr. Mourad Debbabi, Dean
Faculty of Engineering and Computer Science

Abstract

Novel Channel Estimation Methods for GFDM Systems in High Mobility Scenario

Hamidreza Shayanfar

High-mobility wireless environments—such as those experienced in vehicular or aerial networks—pose significant challenges to reliable communication. Rapid time variations and frequency dispersion in these environments lead to severe intersymbol interference and signal distortion. Conventional modulation schemes and channel estimation methods, which are often based on a time-frequency representation, struggle to maintain performance under such conditions. Generalized Frequency Division Multiplexing (GFDM) has emerged as a promising modulation technique for next-generation wireless networks due to its flexibility and efficient spectrum usage. However, its conventional formulation does not adequately address the dynamic nature of high-mobility channels.

This thesis presents a novel approach that redefines the GFDM system model in the delay-Doppler domain. The delay-Doppler domain offers a natural framework for representing channels in high-mobility scenarios, as it captures the sparse structure of the channel more effectively than the conventional time-frequency domain. By transforming the GFDM signal into the delay-Doppler domain, our method exploits the inherent sparsity of the channel, thereby enabling more accurate and efficient channel estimation. Additionally, a superimposed pilot scheme is introduced, whereby pilot symbols are embedded within the data-bearing frame. This strategy eliminates the need for dedicated pilot-only regions, thus significantly enhancing spectral efficiency.

Based on the new system model, we investigate two channel estimation methods. The first approach employs a compressed sensing technique using the Subspace Pursuit (SP) algorithm. This method reconstructs the channel vector from a limited number of measurements, leveraging the

sparse nature of the channel. It offers low computational complexity, which is beneficial for real-time implementations. However, the SP algorithm requires prior knowledge of the channel's sparsity level—a parameter that is often difficult to determine in practice.

To overcome this limitation, the second method adopts Sparse Bayesian Learning (SBL) for channel estimation. SBL integrates prior information about the channel's sparse structure directly into a Bayesian inference framework, allowing it to both accurately estimate the key channel parameters and identify the positions of the non-zero elements without requiring a priori sparsity knowledge. Simulation results demonstrate that the SBL-based estimator outperforms the SP algorithm, particularly in scenarios where pilot overhead is constrained.

Building on these estimation techniques, the thesis further extends the proposed framework to incorporate reconfigurable intelligent surfaces (RIS). RIS are composed of numerous passive reflecting elements that can dynamically adjust their reflection coefficients. By optimizing these coefficients, the RIS can steer the reflected signals to constructively combine with the direct path, thereby enhancing the overall channel gain and system capacity. Hence, a low-complexity phase optimization strategy is then employed to tune the RIS phase coefficients, maximizing the effective channel gain and improving the achievable rate.

The extensive simulation results presented in this thesis validate the performance of the proposed methods. Our findings indicate that the new GFDM system model in the delay-Doppler domain leads to significant improvements in channel estimation accuracy and robustness in high-mobility scenarios. The superimposed pilot scheme enhances spectral efficiency by embedding pilot symbols within the data frame, and the SBL-based channel estimator demonstrates superior performance over conventional greedy methods such as SP. Moreover, the integration of RIS with optimized phase shifts further increases the achievable rate and overall system capacity compared to systems with random phase configurations or without RIS support.

Acknowledgments

First and foremost, I would like to extend my heartfelt gratitude to my thesis supervisors, Dr. M. N. S. Swamy and Dr. Wei-Ping Zhu, for providing me with the opportunity to pursue my master's studies at Concordia University and for guiding me in my academic research. Their unwavering support, valuable insights, and continuous encouragement have been instrumental in the successful completion of this thesis.

I am deeply grateful to my parents for their endless love and support throughout my life, which have been the foundation of all my achievements. I would also like to express my sincere thanks to my wife, whose constant inspiration and support have sustained me throughout my studies.

Contents

List of Figures	viii
List of Tables	x
List of Symbols	xi
1 Introduction	1
1.1 Research Background	1
1.2 Literature Review	3
1.3 Motivation and Objectives	6
1.4 Contributions of the Thesis	8
1.5 Organization of the Thesis	9
2 GFDM-Based Systems	10
2.1 Introduction	10
2.2 Wireless Communication Channels	11
2.2.1 Frequency and Time Selective Channels	11
2.2.2 Delay-Doppler Domain Channels	14
2.3 New Representation of GFDM System in Doubly Selective Channels	16
2.3.1 GFDM System Model in Frequency Selective Channels	16
2.3.2 GFDM System Model in delay-Doppler Domain	20
2.4 Conclusion	22

3	Compressed Sensing Based Channel Estimation for GFDM systems in High Mobility	23
	Scenario	23
3.1	Introduction	23
3.2	Compressed Sensing	24
3.2.1	Principles of Compressed Sensing	25
3.2.2	Subspace Pursuit (SP) Algorithm	26
3.3	Proposed Chanel Estimation using Subspace Pursuit	28
3.4	Simulations	36
3.5	Conclusion	39
4	Sparse Bayesian Learning Channel Estimation in RIS-aided GFDM Systems	41
4.1	Introduction	41
4.2	RIS-aided System Model	42
4.3	Proposed Channel Estimation with Sparse Bayesian Learning	46
4.3.1	Channel Estimation Algorithm	46
4.3.2	A Low-Complexity Scheme with RIS Phase Optimization	51
4.4	Simulations	52
4.5	Conclusion	56
5	Conclusion and Future Work	57
5.1	Conclusion	57
5.2	Future Work	59
	References	61

List of Figures

Figure 2.1	An illustration of frequency-selective, time-selective, and doubly-selective channel models.	13
Figure 2.2	LTV channels in the time-delay, time-frequency, and delay-Doppler domains [30].	15
Figure 2.3	The delay-Doppler vs. LTV time-frequency channel response [31].	15
Figure 2.4	The delay-Doppler vs. LTI time-frequency channel response [31].	16
Figure 2.5	Time-frequency resource block of a GFDM system [33].	18
Figure 2.6	New representation of GFDM system model in the delay-Doppler domain.	22
Figure 3.1	Illustration of a sparse signal \mathbf{x}_s and its measurement vector.	25
Figure 3.2	The block diagram of the new GFDM transceiver. All dotted blocks are associated with the channel estimation and data detection.	31
Figure 3.3	The discrete delay-Doppler grid for input and output matrix of data arrangement block. (a): The input of data arrangement block (i.e. the matrix \mathbf{D}_d). N_r zero rows are distributed with period of Q when \mathbf{E} is considered as (25). (b): Applying the row switching operation and distributing the data symbols inside the pilot-guard frame to the zeros symbols outside of this frame (Here, consider $N_r = 2$, $N_P = 4$ and $M_P = 6$ to explain further how this data spreading is performed.)	33
Figure 3.4	(a) The GFDM frame in the delay Doppler domain with pilots and guard intervals. (b) The symbols used in the channel estimation and data detection parts at the receiver side. Assume $l_{\max} = k_{\max} = 1$, $N_P = 4$ and $M_P = 6$	34

Figure 3.5	The absolute value of each element in the matrix \mathbf{W} (Raised cosine (RC) filter with a roll-ff factor of 0.5) in the delay-Doppler domain, for $M = N = 57$.	34
Figure 3.6	MSE performance comparison of the proposed method at different speeds versus MVU estimator.	37
Figure 3.7	MSE performance comparison among the proposed SP-based channel estimator and the theoretical benchmarks (CRB and Oracle-MMSE) at an SNR of 10 dB, where $M_p = N_p$ and $k_{\max} = l_{\max}$.	38
Figure 3.8	BER performance comparison of the proposed method versus perfect knowledge of the channel available at the receiver side.	39
Figure 4.1	Primary functions of RIS in wireless channel reconfiguration [51].	43
Figure 4.2	RIS-assisted GFDM system with a single-antenna user and BS.	44
Figure 4.3	The transmission protocol; (a) $N_{\text{RIS}} + 1$ pilot symbols for the training phase followed by pure data symbols. (b) One of the pilot symbols considered in the training phrase. Assume $l'_{\max} = k'_{\max} = 1$, $N_P = 5$ and $M_P = 7$.	47
Figure 4.4	MSE performance comparison between the proposed SBL-based channel estimator and the SP algorithm at a Doppler speed of 160 km/h.	54
Figure 4.5	MSE performance comparison among the proposed SBL-based channel estimator, the SP algorithm, and the theoretical benchmarks (CRB and Oracle-MMSE) at an SNR of 10 dB, where $M_p = N_p$.	54
Figure 4.6	Achievable rate for three scenarios: optimized RIS phase selection, random RIS phase selection, and without RIS, with 100 RIS elements.	55
Figure 4.7	Achievable rate versus the number of RIS elements at an SNR of 10 dB.	55

List of Tables

Table 3.1 Simulation Parameters for SP-based Algorithm 36

Table 4.1 Simulation Parameters for SBL-based algorithm 53

List of Symbols

N	Number of subcarriers
M	Number of subsyms
f_c	Carrier frequency
l	Delay tap
k	Doppler tap
P	Number of dominant path
\mathbf{x}^H	Complex Conjugate Transpose of \mathbf{x}
\mathbf{F}_S	S -point normalized discrete Fourier transform (DFT) matrix
\mathbf{I}_S	Identity matrix of size $S \times S$
$\mathbf{1}_S$	All-ones matrix of size $S \times S$
$\mathbb{E}\{\mathbf{x}\}$	Expectaion of \mathbf{x}
$\text{vec}\{\mathbf{X}\}$	Vectorization of a matrix \mathbf{X}
$\langle \cdot \rangle_N$	Modulo- N operator
$\lceil x \rceil$	Smallest integer that is no smaller than x
\otimes	Kronecker product
$ \mathbf{x} $	Absolute Value of the Elements of \mathbf{x}
$\ \mathbf{x}\ $	Euclidean distance of the vector of \mathbf{x}

Chapter 1

Introduction

1.1 Research Background

Over the past decade, wireless communication systems have evolved at an unprecedented pace to meet growing demands for higher data throughput, broader coverage, and more reliable connectivity. These demands arise from the growth of data-intensive applications such as high-definition video streaming, interactive online gaming, and real-time data sharing, all of which require robust and seamless network performance. As a result, service providers and system designers face the dual challenge of maintaining consistent service quality while managing the growing complexity of modern wireless networks[1].

The transition from 4G to 5G technologies marked a milestone in this evolution, featuring innovations in network architectures, spectrum utilization strategies, and signal processing techniques. In particular, 5G introduced capabilities such as massive Multiple-Input Multiple-Output (MIMO) and millimeter-wave transmissions, enabling significant improvements in capacity and coverage [2]. Meanwhile, ongoing research into 6G technologies aims to further expand these boundaries by addressing emerging requirements such as ultra-low latency, enhanced energy efficiency, and massive machine-type communications [1].

A key waveform technology employed in many current wireless standards (e.g., LTE, Wi-Fi (IEEE 802.11), and 5G NR) is Orthogonal Frequency Division Multiplexing (OFDM) [3]. By dividing the available bandwidth into numerous narrow subcarriers, OFDM simplifies receiver design

through single-coefficient equalization per subcarrier. The intrinsic orthogonality of these subcarriers also reduces inter-carrier interference under ideal conditions, resulting in high spectral efficiency and making OFDM highly suitable for applications demanding large data rates and robust performance.

Despite its advantages, OFDM faces significant challenges in high-mobility environments—such as vehicular communications, high-speed trains, and aerial networks—where rapid channel variations and Doppler effects complicate channel estimation [4]. In these scenarios, the channel coherence time is drastically reduced, and Doppler shifts can destroy the subcarriers' orthogonality, leading to increased inter-carrier interference (ICI) and degraded system performance. Additionally, OFDM signals often exhibit a high peak-to-average power ratio (PAPR), requiring power amplifiers with a large dynamic range and reduced power efficiency [5]. Although advanced signal processing techniques and pilot designs can partially mitigate these issues, they become increasingly complex and less effective as mobility increases.

In response to these challenges, researchers have investigated alternative waveforms and new signal processing paradigms that can better handle fast-varying channels and improve channel estimation accuracy under mobility constraints. Among these, Generalized Frequency Division Multiplexing (GFDM) has gained significant attention as a promising candidate for next-generation wireless systems [6]. Unlike OFDM, GFDM relaxes the requirement for strict orthogonality among subcarriers, instead employing a non-orthogonal waveform structure with pulse-shaped subcarriers. This approach offers multiple benefits: reduced out-of-band (OOB) emissions, potentially lower PAPR, and improved robustness to Doppler shifts.

Nevertheless, GFDM's non-orthogonality introduces new challenges for channel estimation, since interference among subcarriers is no longer inherently mitigated by strict orthogonality. In high-mobility scenarios, where the channel can vary significantly over short time intervals, designing effective pilot patterns and developing reliable estimation algorithms become even more complex. Effective channel estimation techniques for GFDM must account for the interplay between pulse shaping, Doppler spread, and time-varying fading, while minimizing the overhead required for pilot transmission. This makes GFDM a particularly rich and active area of research, especially for applications involving rapid mobility.

Consequently, the exploration of robust channel estimation strategies for GFDM systems is critical to unlocking their full potential in future wireless networks. By effectively tracking channel variations and mitigating interference, GFDM can realize higher throughput and more reliable connectivity under the stringent conditions of high-speed mobility. As such, advanced channel estimation techniques for GFDM not only address the limitations of OFDM in these scenarios but also pave the way for more efficient and flexible multi-carrier communication systems.

1.2 Literature Review

Channel estimation plays a crucial role in the performance of wireless communication systems, where accurately determining channel characteristics can significantly affect the reliability and efficiency of data transmission. In the context of GFDM systems, traditional channel estimation techniques [7, 8, 9, 10] have been designed with low-mobility scenarios in mind, where channel conditions vary minimally during a transmission frame. In such environments, classical approaches such as [7, 9], typically assume slow channel variations, enabling effective estimation with minimal complexity and overhead. However, in high mobility scenarios, conventional channel estimation techniques, which assume relatively constant channel characteristics throughout a frame, may become ineffective. The application of such methods in high mobility scenarios can lead to challenges such as increased computational complexity and reduced spectral efficiency due to the rapid variation in channel conditions over a symbol period. Recently, there have been a few studies aiming to estimate time-varying channels for GFDM systems, such as [11, 12]. These approaches often require the channel to be estimated and detected through interpolation and prediction at the data symbols. However, they generally do not account for the sparse properties of the channel, which could otherwise be leveraged for more efficient estimation.

Recently, a new modulation scheme known as Orthogonal Time Frequency Space (OTFS) has been introduced specifically to address the challenges posed by high mobility environments [13]. OTFS operates in the delay-Doppler domain and is designed to convert a time-varying channel into a quasi-static one for the duration of a transmission frame [14]. This unique capability ensures that

the channel gain remains constant across all symbols within a frame, simplifying the channel estimation process and enhancing system robustness under high mobility scenarios. Exploiting this stability, specialized estimation methods have been explored [15, 16, 17]. Research documented in [15] used threshold-based channel estimation with a single pilot impulse, but this method is highly sensitive to noise and increase the peak-to-average power ratio. To enhance estimation accuracy, more sophisticated pilot arrangements have been proposed in [16], where multiple pilots transform channel estimation into a sparse recovery problem tackled by three-dimensional orthogonal matching pursuit (OMP). This approach, however, as part of an OFDM-based OTFS modulation framework, introduces additional pilot symbols for channel estimation, thereby increasing overhead. Further refinements involve sparse Bayesian algorithms to capture both integer and fractional parts of Doppler [17], again at the cost of additional guard symbols and reduced spectral efficiency.

Despite the effectiveness of OTFS in handling time-varying channels, directly applying these techniques to GFDM systems is difficult, as OTFS relies on an underlying OFDM-based structure. This necessitates the development of novel channel estimation approaches tailored for GFDM systems that operate in the delay-Doppler domain in high mobility scenarios. Although OTFS demonstrates strong Doppler resilience, GFDM remains an attractive option in moderate to high mobility scenarios due to its flexible subcarrier pulse shaping, which can address high out-of-band (OOB) emissions and large PAPR problems often seen in rectangular pulse-shaping filters [18, 19], which is the common filter employed in the literature for the OTFS systems

While OTFS is particularly advantageous in high-mobility environments due to its robustness against Doppler effects, GFDM performs effectively in moderate mobility scenarios, making it a suitable choice for applications where channel conditions are less severe [20]. Furthermore, the rectangular pulse shaping filter, which may lead to high OOB emissions and large PAPR [18], is the common waveform employed in the literature for the OTFS systems. However, due to the flexibility in prototype pulse shape configuration, GFDM can employ tailored pulse shaping filters to mitigate out-of-band emissions and reduce PAPR, thereby enhancing spectral efficiency and power efficiency [19]. This distinction highlights the need for specialized adaptations in GFDM channel estimation techniques to fully leverage its potential in varying mobility conditions, bridging the gap between traditional and novel approaches in the field.

Another emerging area in wireless communication research involves the integration of Reconfigurable Intelligent Surfaces (RIS) with traditional communication systems such as GFDM to further enhance performance, especially in complex channel environments. RIS has the potential to significantly improve the spectral and energy efficiency of communication systems. Existing channel estimation methods for RIS generally fall into two categories: separate channel estimation and cascaded channel estimation [21]. For the former, based on the received pilots, the channels from the BS/users to the RIS can be obtained separately at some sensing elements mounted on the RIS. Accurate channel estimation in this way is a key challenge due to the limited number of sensing components. Although compressed sensing can help overcome the limited number of sensing components [22], the optimal distribution of these elements and the associated algorithms remain open challenges [21]. On the other hand, in the cascade method, because there are no more such sensing components on the RIS, the channel from BS/user to the RIS can not be estimated separately. There are many studies on the cascade estimation in the literature. Early methods turned on one RIS element at a time to measure its contribution [23], while subsequent work employed full-ON RIS reflection patterns or more sophisticated compressed sensing approaches to reduce the number of required time slots [24, 25, 26]. In particular, in [24], the authors propose a practical transmission protocol for RIS-enhanced OFDM systems, introducing an RIS reflection pattern to facilitate channel estimation at the access point using uplink pilot signals. Based on the estimated CSI, they optimize RIS reflection coefficients with a low-complexity algorithm that maximizes the strongest time-domain signal path, achieving near-optimal performance with reduced computational complexity. In [25], the authors propose two fast channel estimation schemes for RIS-assisted OFDM: one reduces training time by shortening OFDM symbols, while the other exploits sampling-wise RIS reflection variation for enhanced accuracy, particularly in LoS-dominant channels. In [26], the authors propose a hybrid large intelligent surfaces (LIS) architecture with a few active elements to reduce training overhead and hardware complexity. They developed two solutions: a compressive sensing-based method to reconstruct full LIS channels and a deep learning-based approach to directly predict optimal reflection matrices. While these studies reveal considerable progress in RIS channel estimation, their focus is predominantly on OFDM-based systems or other standard waveforms in low-mobility settings. Investigations on RIS-enhanced GFDM [27] have similarly been

limited to scenarios with minimal Doppler effects, leaving high mobility scenarios unexplored. The ability of RIS to dynamically alter the propagation environment presents a novel opportunity to enhance GFDM systems, yet it also complicates channel estimation significantly. This indicates a pressing need for innovative research to develop new channel estimation techniques that can harness the reconfigurable nature of RIS to optimize performance in high mobility settings.

1.3 Motivation and Objectives

In practical wireless communication, channels are far from ideal. Signals face attenuation and distortion due to multipath effects. These issues are more challenging in high mobility scenarios like in high-speed vehicles or trains, where the channel conditions can change rapidly. Traditional methods of boosting the signal power are insufficient for overcoming these challenges. Therefore, precise channel estimation and equalization are crucial for maintaining reliable communication under such conditions.

Traditional channel models, such as those based on time-frequency representations, often assume a relatively static environment where the multipath components vary slowly. These models can become overly complex and computationally intensive in high mobility scenarios because they must account for frequent, significant variations in the channel's characteristics. One effective method to tackle the rapid changes in the channel is to represent it in the delay-Doppler domain, where the channel's characteristics are naturally sparse. This sparsity arises because only a few paths dominate due to the high Doppler shifts associated with high mobility. Exploiting this inherent channel sparsity can enable more efficient and rapid estimation techniques, significantly improving performance under fast time-varying conditions.

To effectively work with the delay-Doppler channel model, it is essential to adapt the multicarrier system model to a representation in the delay-Doppler domain. One such approach involves transforming the GFDM system, which is traditionally represented in the time-frequency domain, into the delay-Doppler domain. This transformation is crucial because GFDM, in its conventional form, focuses on managing inter-carrier interference and maximizing spectral efficiency within a static or slowly varying channel environment. By representing GFDM in the delay-Doppler domain,

the system can better accommodate and exploit the sparsity of the channel in scenarios characterized by high mobility. This adaptation not only aligns the system model with the physical realities of the channel but also enhances the system's ability to handle rapid variations in the channel dynamics, leading to more robust and efficient communication in high mobility environments.

Additionally, another innovative method to enhance communication systems involves the use of RIS. RIS consist of numerous programmable elements that can manipulate the phase and amplitude of incoming electromagnetic waves, allowing precise control over the wavefront. Specifically, RIS can establish a virtual line-of-sight (LOS) link between transceivers, effectively bypassing obstacles through smart reflections. This capability not only adds more signal paths in the desired direction to improve the channel rank condition but also refines the channel statistics and suppresses interference, thereby enhancing overall communication quality. However, while RIS can significantly improve signal propagation and reception, their integration introduces new complexities into the channel estimation process. The dynamic nature of RIS elements adds additional variables to the channel model, thereby increasing the difficulty of accurately modeling and adapting to changes in the propagation environment. Addressing these challenges is essential, as advanced channel estimation methods are required to harness the full potential of RIS without affecting system performance.

By exploiting the delay-Doppler domain representation and integrating RIS capabilities, the objective of this thesis is to develop advanced channel estimation and equalization techniques for GFDM systems in high-mobility environments. Specifically, the objective is to design methods that take advantage of channel sparsity, using compressed sensing techniques and Bayesian learning, to achieve efficient and robust performance despite rapid channel variations. In addition, the thesis will explore new strategies for incorporating RIS into these systems to further improve signal propagation and establish reliable virtual line-of-sight links. Through these contributions, the work seeks to enhance the adaptability and overall quality of next-generation wireless communication systems, especially in scenarios characterized by frequent and significant changes in channel conditions.

1.4 Contributions of the Thesis

This thesis presents several notable contributions to wireless communication research, particularly in high-mobility scenarios. These contributions have also led to two conference papers derived from the core findings of this work. References to these papers are provided after the relevant contribution points listed below.

- (1) **New Representation of the GFDM System in the Delay-Doppler Domain:** A new model of the GFDM system is formulated in the delay-Doppler domain [28]. By leveraging the channel’s inherent sparsity under high-mobility conditions, this representation enables more efficient channel estimation and improved system performance in rapidly changing environments.
- (2) **Superimposed Pilot Symbols Embedding:** To boost spectral efficiency, we introduce a strategy for embedding superimposed pilot symbols within GFDM data frames. By eliminating the need for separate pilot frames, the proposed method reduces overhead and maximizes effective bandwidth utilization [28].
- (3) **Compressed Sensing Channel Estimation Using Sparse Priors:** Building on the sparse characteristics of the delay-Doppler channel, this work employs compressed sensing techniques—specifically Subspace Pursuit (SP)—for robust channel estimation. This approach minimizes both the number of measurements and the computational burden, making it particularly suitable for fast time-varying channels [28].
- (4) **Integration of RIS Panels and Bayesian Learning for Channel Estimation:** To further enhance communication quality, RIS panels are deployed in the communication system. A Bayesian learning approach is adopted to perform channel estimation for the RIS-aided systems. This method aims to address the complexities introduced by RIS and provides a robust framework for characterizing and optimizing the modified propagation environment [29].

These contributions not only address some of the fundamental challenges in high mobility wireless communications but also pave the way for more efficient and reliable communication technologies. By exploring new system models, innovative pilot embedding techniques, and advanced

channel estimation methods, this thesis advances the state of the art in adapting wireless systems to the demands of rapidly changing environments.

1.5 Organization of the Thesis

The remainder of this thesis is structured as follows: Chapter 2 provides the theoretical foundation for wireless communication channels, beginning with frequency-selective and doubly-selective (time-varying) channel models. It then reviews the conventional GFDM system model and introduces a novel approach to represent GFDM in the delay-Doppler domain, laying the groundwork for improved channel estimation in high-mobility scenarios. In chapter 3 we focus on the proposed channel estimation technique using the new delay-Doppler GFDM framework. In particular, a compressed sensing method is presented to leverage the channel's sparsity for efficient estimation. Subsequently, in chapter 4 the integration of RIS into GFDM is explored, and a Sparse Bayesian Learning approach is introduced to handle the added complexity of RIS-enabled propagation paths. Finally, Chapter 5 concludes the thesis by summarizing the key findings and their implications for high-mobility wireless systems. It also outlines potential directions for future work, including advanced optimizations for RIS-assisted GFDM and further exploration of robust channel estimation methods in complex propagation environments.

Chapter 2

GFDM-Based Systems

2.1 Introduction

Wireless communication systems must deal with varying channel conditions that can significantly affect their performance. Among these, frequency-selective channels, where different frequency components of a signal experience varying degrees of fading, pose substantial challenges in achieving reliable data transmission. Furthermore, in high mobility environments, these channels often exhibit doubly-selective behavior, where both time and frequency selectivity must be addressed simultaneously. These time-varying channels are characterized by rapid changes in multipath components, leading to increased complexity in signal processing tasks at the receiver such as equalization and channel estimation. To better understand these challenges, this chapter begins by providing an overview of frequency-selective and delay-Doppler channel models, detailing their mathematical representation and the implications for modern communication systems. This chapter then shifts focus to the GFDM system, beginning with a detailed review of its conventional time-frequency domain model, including its design principles, strengths, and limitations. While traditional GFDM performs well in low-mobility environments, it struggles to handle the rapid channel variations characteristic of doubly-selective channels. These challenges highlight the need for enhanced system models and advanced signal processing techniques optimized for high-mobility scenarios. To address this, the chapter concludes by proposing a novel representation of the GFDM

system in the delay-Doppler domain, leveraging channel sparsity to improve performance in high-mobility conditions.

2.2 Wireless Communication Channels

In this section, we explore the foundational concepts of wireless communication channels, which are crucial for understanding the behavior and performance of wireless communication systems. We start by introducing frequency fading channels, providing insight into the challenges posed by the multipath propagation effects, where signals take multiple paths of varying lengths to reach the receiver. Following this, we explore doubly selective channels that exhibit variations both in time and in frequency. This discussion is essential for understanding the delay-Doppler representation, an essential framework for designing communication systems that can perform effectively in high-mobility scenarios.

2.2.1 Frequency and Time Selective Channels

Frequency-selective channels, also referred to as frequency-fading channels, are a fundamental concept in wireless communication, where the channel's frequency response varies significantly across the bandwidth of the signal. This variation arises primarily from multipath propagation, where transmitted signals traverse multiple paths of differing lengths before reaching the receiver. Each path introduces a unique delay, causing time dispersion and frequency-selective fading in the received signal. As a result, different frequency components of the signal experience varying levels of attenuation and phase shift, making frequency-selective channels a critical consideration in the design and optimization of wireless communication systems.

To fully understand frequency-selective channels, it is essential to describe their behavior in terms of the channel impulse response (CIR) in the delay domain, denoted as $h(\tau)$. The CIR characterizes the time-dispersive nature of the channel by describing how an input signal is spread over time as it travels through the channel. The relationship between the CIR and the frequency-selective behavior of the channel is captured by its channel transfer function (CTF) in the frequency domain. The CTF, denoted by $H(f)$, is derived as the Fourier Transform (FT) of the CIR, mathematically

expressed as

$$H(f) = \int_{-\infty}^{\infty} h(\tau) e^{-j2\pi f\tau} d\tau. \quad (1)$$

This frequency-domain representation illustrates how different frequency components of the signal are attenuated or phase-shifted due to the channel. The frequency selectivity of the channel is primarily determined by the delay spread of the CIR, denoted by τ_d , which reflects the range over which significant multipath components arrive. The relationship between the delay spread and the coherence bandwidth B_c of the channel can be approximated as $B_c \approx \frac{1}{\tau_d}$. A larger delay spread results in a smaller coherence bandwidth, indicating that the channel's frequency response changes more rapidly across the signal's spectrum. This results in severe intersymbol interference (ISI) as different frequency components of the signal experience different gains and delays. Without effective mitigation strategies, selective fading across the channel's bandwidth can severely degrade communication reliability and performance.

In wireless communication systems, the assumption of a linear time-invariant CIR is often valid in scenarios where the channel exhibits long coherence times and minimal variations. However, this assumption fails in high-mobility environments or at higher carrier frequencies, where the channel instead exhibits linear time-variant (LTV) characteristics. As a result, the LTV channel model has attracted significant research interest due to its relevance in dynamic and rapidly changing propagation environments. An LTV channel introduces frequency shifts caused by the Doppler effect, which leads to a spectral-smeared version of the transmitted signal. This phenomenon makes the channel frequency-dispersive, with the degree of dispersion directly proportional to the Doppler spread. The relationship between the Doppler spread, f_d , and the coherence time, T_c , is given by $T_c \approx \frac{1}{f_d}$, where f_d denotes the maximum Doppler frequency. The time-selective nature of frequency-dispersive channels arises from the rapid fluctuations in the channel's time-domain fades, with these fluctuations becoming more pronounced and increasingly separated as the Doppler spread increases.

In practice, high-mobility scenarios often give rise to doubly dispersive channels due to the combined effects of multipath propagation and the Doppler effect, as illustrated in Fig. 2.1. This channel is characterized by variations in both time and frequency, making them significantly more

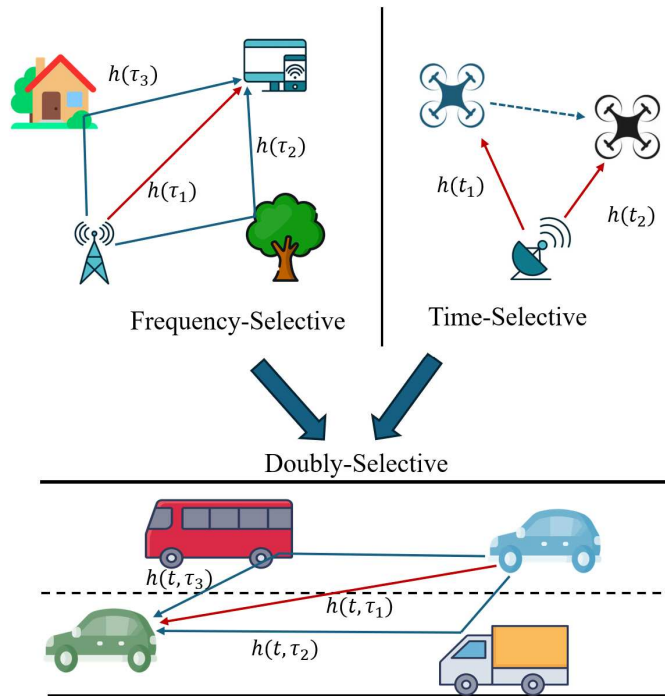


Figure 2.1: An illustration of frequency-selective, time-selective, and doubly-selective channel models.

complex to model and analyze than frequency-selective or time-selective channels alone. The time-varying CIR, denoted as $h(\tau, t)$, captures both the temporal and spectral dynamics of the channel, where τ represents the delay dimension and t corresponds to time.

In doubly selective channels, the simultaneous presence of time dispersion (caused by multipath propagation) and frequency dispersion (resulting from Doppler shifts) leads to severe signal impairments. These include ISI, due to overlapping multipath components in the delay domain, and inter-carrier interference (ICI), caused by the loss of orthogonality between subcarriers in the frequency domain. These impairments pose significant challenges to signal reception and require sophisticated equalization and channel estimation techniques to mitigate their effects. Despite their complexity, doubly dispersive channels in high-mobility environments also introduce additional degrees of freedom, which can be exploited to enhance communication reliability. By leveraging these degrees of freedom through diversity-aided techniques, such as delay-Doppler domain processing or advanced modulation schemes, it is possible to achieve improved performance even under challenging conditions.

2.2.2 Delay-Doppler Domain Channels

LTV channels, while often represented in the time-delay domain, can also be equivalently described in the time-frequency or delay-Doppler domains. Each of these representations provides unique insights into the channel's characteristics and plays a critical role in designing communication systems for different scenarios.

The time-frequency domain channel, denoted as $h(t, f)$, is derived by applying the Fourier Transform of $h(t, \tau)$ with respect to the delay variable τ . This representation highlights the channel's frequency selectivity and time-variant behavior, where $h(t, f)$ describes the channel transfer function (CTF) at a specific time t and frequency f . However, in high-mobility scenarios, the coherence time and coherence bandwidth of the LTV channel, which define the limits of its stability in time and frequency, are significantly reduced. As illustrated in Fig. 2.2, the coherence region in the time-frequency domain is relatively small for such channels, necessitating frequent updates to track their dynamics. This results in substantial signaling overhead and increased computational demands, which complicates the application of time-frequency-based models in highly dynamic environments.

In contrast, the delay-Doppler domain channel is obtained by applying the Fourier Transform of $h(t, \tau)$ with respect to time t , yielding $h(\tau, \nu)$. In this representation, $h(\tau, \nu)$ describes the channel's scattering function, capturing the contributions of scatterers with specific propagation delays τ and Doppler frequency shifts ν . The delay-Doppler domain is particularly advantageous for modeling LTV channels, as it reveals several beneficial features, such as separability, stability, compactness, and often sparsity, as depicted in Fig. 2.2. These features make the delay-Doppler domain highly suitable for addressing the challenges posed by high-mobility scenarios.

- Separability and Stability: The delay-Doppler domain allows the channel's delay and Doppler dimensions to be processed independently, enabling more efficient signal processing and channel estimation techniques.

- Sparsity: In many practical scenarios, only a small subset of scatterers dominates the channel, resulting in a sparse representation in the delay-Doppler domain. This sparsity can be exploited to reduce computational complexity, signaling overhead, and pilot requirements, thereby enhancing

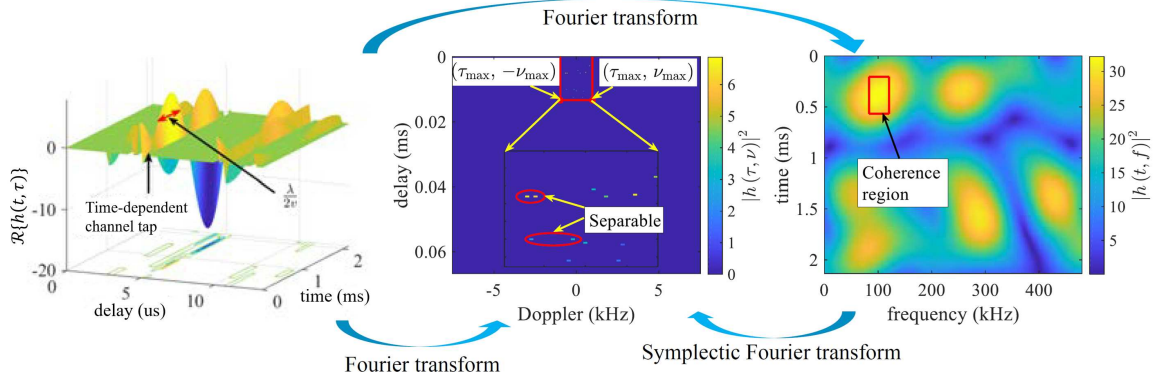


Figure 2.2: LTV channels in the time-delay, time-frequency, and delay-Doppler domains [30].

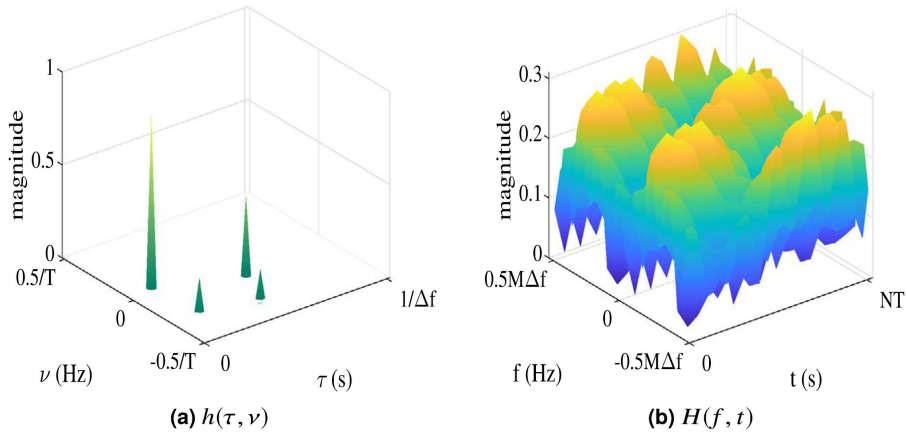


Figure 2.3: The delay-Doppler vs. LTV time-frequency channel response [31].

system performance.

Fig. 2.3 and Fig. 2.4 show a comparison between the delay-Doppler domain on the one hand and LTI and LTV time-frequency channel response on the other hand. As shown in these figures, while the channel in the delay Doppler domain can be considered sparse, in the LTV time-frequency channel response, more time-frequency coefficients are required to represent the channel accurately [31]. By leveraging the properties of the delay-Doppler domain, it becomes possible to design communication systems that are more robust to rapid channel variations. This representation not only simplifies the mathematical modeling of LTV channels but also opens up opportunities for advanced techniques in channel estimation, system optimization, and efficient resource allocation.

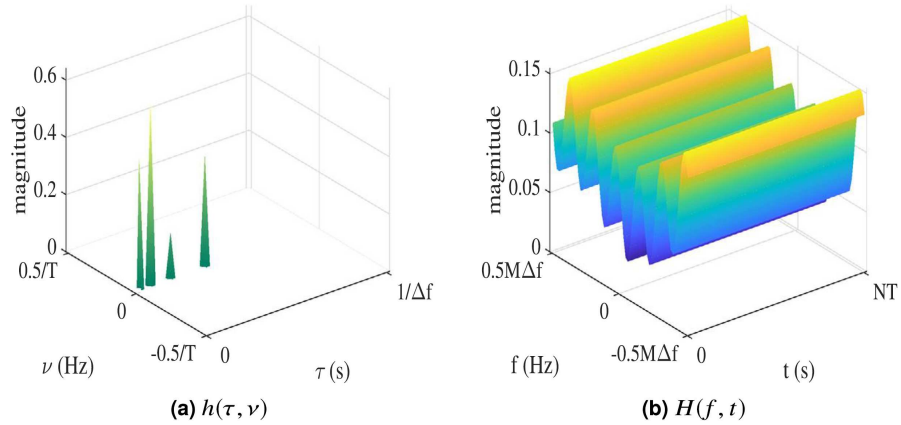


Figure 2.4: The delay-Doppler vs. LTI time-frequency channel response [31].

2.3 New Representation of GFDM System in Doubly Selective Channels

As we update our approach to modeling channels for high-mobility environments, it's important to reconsider how we use modulation techniques like GFDM, which is usually defined in the time-frequency domain. To fully exploit the sparsity properties of channels in high-mobility scenarios, it is essential to redefine the GFDM system in the delay-Doppler domain as well. This approach not only aligns with the evolving needs of modern wireless communication systems but also enhances the system's performance by leveraging the sparse nature of the delay-Doppler domain. The forthcoming sections will detail the traditional time-frequency domain representation of the GFDM system, followed by introducing a novel representation in the delay-Doppler domain, highlighting how this can be beneficial in rapidly changing channels.

2.3.1 GFDM System Model in Frequency Selective Channels

GFDM is a flexible and efficient modulation scheme designed to meet the demands of next-generation wireless networks. Its inherent configurability and efficient utilization of the frequency spectrum make it particularly well-suited for addressing the challenges of frequency-selective channels.

In a conventional GFDM system, MN data symbols $d_{n,m}$ ($n = 0, \dots, N - 1$ and $m =$

$0, \dots, M - 1$) are generated by mapping binary data into complex-valued Quadrature Amplitude Modulation (QAM) symbols. These symbols are transmitted over a time-frequency resource block, which consists of M subsymbols and N subcarriers, as illustrated in Fig. 2.5. The discrete base-band transmit signal in a GFDM system is constructed as the summation of all subcarriers and subsymbols, expressed mathematically as [20]:

$$s[q] = \sum_{n=0}^{N-1} \sum_{m=0}^{M-1} d_{n,m} g_{n,m}[q], \quad (2)$$

where $q = 0, \dots, MN - 1$. The transmit filter $g_{n,m}[q]$ is given by:

$$g_{n,m}[q] = g[\langle q - mN \rangle_{MN}] e^{j2\pi nq/N}, \quad (3)$$

where $g[q]$ is the impulse response of the prototype filter with MN samples, and $\langle \cdot \rangle_{MN}$ denotes the modulo operation that ensures circular shifting. This filter is circularly shifted in both the time and frequency domains and can be represented as a column vector $\mathbf{g}_{n,m}$. The circular convolution created by the modulo operation ensures that the resulting sequence remains of length MN , which is computationally efficient for implementation [32].

The prototype filter, $g[q]$, plays a pivotal role in GFDM systems. Common choices include the Raised Cosine (RC) and Root Raised Cosine (RRC) filters, which are essential for controlling OOB emissions and reducing ICI [33]. These characteristics are particularly beneficial in frequency-selective channels, where multipath propagation can introduce significant distortion. Additionally, the parameters of the prototype filter, such as the roll-off factor β , allow for tuning the trade-off between spectral efficiency and robustness against channel impairments, making GFDM a versatile modulation scheme for a wide range of applications.

Similar to OFDM, a cyclic prefix (CP) is appended to the transmitted signal $s[q]$ in (2) to mitigate ISI caused by multipath propagation. The length of the CP, denoted as N_{CP} , is typically chosen to be longer than the maximum delay spread of the channel. This ensures that each GFDM block can be decoded without interference from adjacent blocks, preserving the integrity of the transmitted data.

The use of circular convolution and flexible pulse-shaping in GFDM makes it highly adaptable

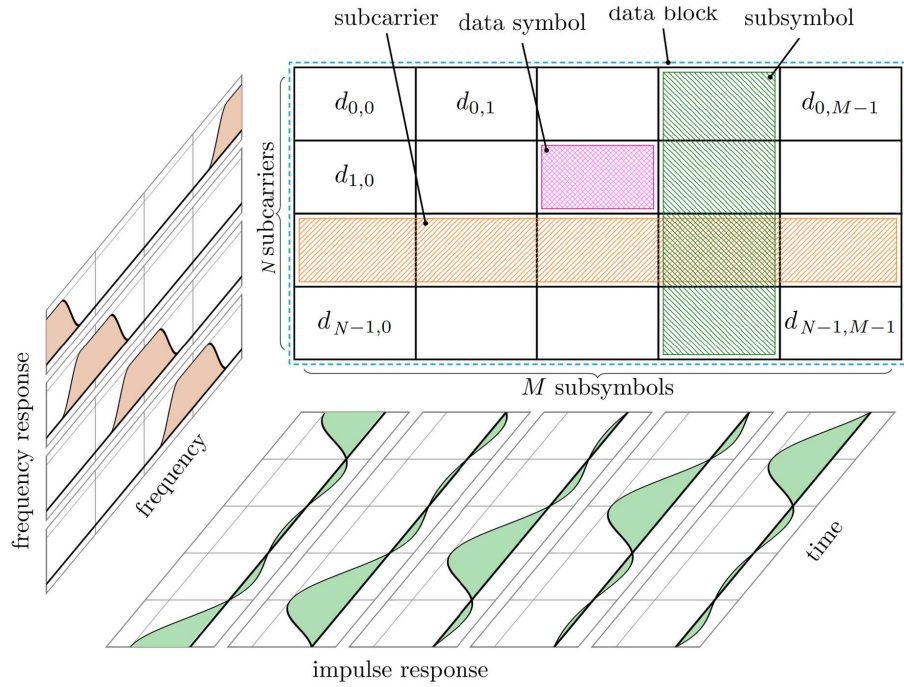


Figure 2.5: Time-frequency resource block of a GFDM system [33].

to various channel conditions. Its ability to manage ICI and reduce OOB emissions positions it as a strong candidate for applications requiring high spectral efficiency and resilience to frequency-selective fading. In contrast to OFDM, GFDM does not require strict orthogonality between subcarriers, allowing for greater flexibility in system design while maintaining robustness in challenging wireless environments.

In matrix notation, the generation of the transmit samples $\mathbf{s} = s[q]^T$ for $q = 0, \dots, MN - 1$ can be expressed as:

$$\mathbf{s} = \mathbf{A}\mathbf{d}, \quad (4)$$

where the data vector \mathbf{d} is arranged as:

$$\mathbf{d} = \left(d_{0,0} \ \cdots \ d_{0,M-1} \ d_{1,0} \ \cdots \ d_{1,M-1} \ \cdots \ d_{N-1,M-1} \right)^T, \quad (5)$$

and the transmit filter matrix \mathbf{A} is given by:

$$\mathbf{A} = \left(\mathbf{g}_{0,0} \ \cdots \ \mathbf{g}_{0,M-1} \ \mathbf{g}_{1,0} \ \cdots \ \mathbf{g}_{1,M-1} \ \cdots \ \mathbf{g}_{N-1,M-1} \right)^T. \quad (6)$$

After transmission through the frequency-selective channel and removal of the CP, the received signal can be expressed as:

$$\mathbf{r} = \mathbf{R}_{\text{CP}} \mathbf{H}_{\text{T}} \mathbf{T}_{\text{CP}} \mathbf{s} + \mathbf{v}, \quad (7)$$

where $\mathbf{v} \sim \mathcal{CN}(0, \sigma^2 \mathbf{I}_{NM})$ represents complex additive white Gaussian noise (AWGN) with variance σ^2 . Here, \mathbf{T}_{CP} and \mathbf{R}_{CP} are the cyclic prefix insertion and removal matrices, respectively. Also, \mathbf{H}_{T} represents the channel matrix, which comprises the CIR elements and facilitates the convolution operation with the transmitted signal. It can be shown that the product $\mathbf{R}_{\text{CP}} \mathbf{H}_{\text{T}} \mathbf{T}_{\text{CP}}$ is equivalent to a circulant matrix \mathbf{H}_{C} . This property simplifies channel equalization, as circulant matrices can be diagonalized using the Discrete Fourier Transform (DFT). Specifically, a circulant matrix can be represented as:

$$\mathbf{H}_{\text{C}} = \mathcal{F}_{MN}^H \mathcal{H} \mathcal{F}_{MN},$$

where \mathcal{F}_{MN} is the DFT matrix, and \mathcal{H} is a diagonal matrix containing the frequency-domain representation of the channel. This diagonalization allows efficient channel equalization using a single-tap frequency-domain equalizer (FDE) [35]. The equalized signal is then given by:

$$\mathbf{s}_{\text{eq}} = \mathcal{F}_{MN}^H \mathcal{H}^{-1} \mathcal{F}_{MN} \mathbf{r} = \mathbf{s} + \mathbf{v}', \quad (8)$$

where \mathbf{v}' is the noise after equalization. To recover the transmitted data \mathbf{d} from the equalized signal \mathbf{s}_{eq} , a minimum mean square error (MMSE) receiver is employed to mitigate the effects of the transmit filter \mathbf{A} on the received signal [36]. This ensures accurate data recovery even in the presence of noise and channel distortions.

So far, we have outlined the method for channel equalization in frequency-selective channels using the conventional GFDM system model. However, in doubly selective channels, where both

time and frequency variations occur, channel estimation and equalization become significantly more challenging. This is because the traditional GFDM system model is not well-suited to handle the additional complexity introduced by time-variant channels. To address these challenges, the next subsection introduces a novel representation of the GFDM system in the delay-Doppler domain. This new representation simplifies channel estimation and equalization in doubly selective channels, leveraging the sparsity and stability of the delay-Doppler domain to enhance performance compared to the conventional system model.

2.3.2 GFDM System Model in delay-Doppler Domain

As mentioned earlier, in doubly selective channels, the channel experiences variations in both time and frequency domains. Consequently, the conventional representation in (7) cannot be directly applied for channel estimation and equalization under these conditions. On the other hand, LTV channels exhibit sparsity in the delay-Doppler domain, making it advantageous to represent the GFDM system in this domain. To exploit this sparsity, we propose a novel representation of the GFDM system model in the delay-Doppler domain, Fig. 2.6. This process involves transforming the time-frequency domain data symbols into the delay-Doppler domain, applying the pulse-shaping filter in this domain, and then transforming the result back to the time domain¹, as illustrated in the transmitter section of the system model in Fig. 2.6. Specifically, let an $N \times M$ matrix \mathbf{D} contain all QAM data symbols $d_{n,m}$, where $n = 0, 1, \dots, N - 1$ and $m = 0, 1, \dots, M - 1$. To transform these symbols from the time-frequency domain to the delay-Doppler domain, we use the symplectic finite Fourier transform (SFFT) [37], defined as:

$$\mathbf{D}_d[l, k] = \frac{1}{\sqrt{NM}} \sum_{n=0}^{N-1} \sum_{m=0}^{M-1} \mathbf{D}[n, m] e^{-j2\pi(\frac{km}{M} - \frac{ln}{N})}, \quad (9)$$

where $l = 0, 1, \dots, N - 1$ and $k = 0, 1, \dots, M - 1$. The SFFT can also be expressed in matrix form as:

$$\mathbf{D}_d = \mathcal{F}_N^H \mathbf{D} \mathcal{F}_M, \quad (10)$$

¹The receiver processing, including the inverse transformations and our proposed channel estimation method, will be discussed in detail in the next chapter.

where \mathcal{F}_N and \mathcal{F}_M represent the DFT matrices of size $N \times N$ and $M \times M$, respectively. Following (2), subcarriers are filtered using the transmit filter. Instead of performing convolution in the time-frequency domain, we apply an element-wise multiplication in the delay-Doppler domain. Specifically, the filtered signal in the delay-Doppler domain is obtained as:

$$\mathbf{X}_{\text{dd}} = \mathbf{D}_d \odot \mathbf{W}, \quad (11)$$

where \mathbf{W} represents the transmit filter in the delay-Doppler domain and is defined as:

$$\mathbf{W} = (N\mathcal{F}_M (\text{unvec}_{N \times M}(\mathbf{g}_{n,m})^{\text{T}}))^{\text{T}}. \quad (12)$$

Here, $\mathbf{g}_{n,m}$ is derived from $g_{n,m}[q]$, as defined in (2). To transform the signal back into the time domain, which is necessary for transmission through the channel, we employ the inverse discrete Zak transform (IDZT) [31], followed by a parallel-to-serial conversion. The transmitted signal \mathbf{s} can then be expressed as:

$$\mathbf{s} = \text{vec}(\mathbf{S}) = (\mathcal{F}_M^{\text{H}} \otimes \mathbf{I}_N)\mathbf{x}_{\text{dd}}, \quad (13)$$

where $\mathbf{S} = \mathbf{X}_{\text{dd}}\mathcal{F}_M^{\text{H}}$, \mathbf{x}_{dd} is the vectorized form of \mathbf{X}_{dd} , \otimes represents the Kronecker product, and \mathbf{I}_N is the identity matrix of size N . Finally, a cyclic prefix (CP) is appended to \mathbf{s} before transmission through the channel. With the help of [20], it can be shown that the signal \mathbf{s} derived in (13) is equivalent to the one obtained in (2), confirming the consistency of this new representation with the conventional time-frequency approach².

This new delay-Doppler domain representation will be utilized in subsequent chapters (3 and 4) to simplify channel estimation and equalization in doubly selective channels by taking advantage of the domain's inherent sparsity. Hence, the proposed system provides a generalized multicarrier framework that can be effectively employed in both low- and high-mobility scenarios, offering advantages such as OOB emissions and PAPR compared to conventional OFDM-based multicarrier systems.

²This new transceiver model is inspired by the framework in [20]. However, we propose a matrix-based system model, which offers a more streamlined and potentially simpler representation than the one in [20].

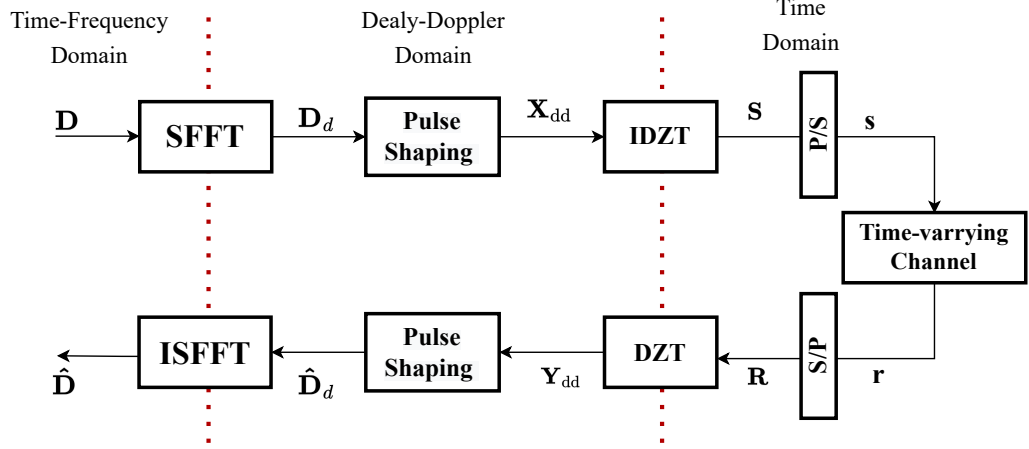


Figure 2.6: New representation of GFDM system model in the delay-Doppler domain.

2.4 Conclusion

In this chapter, we highlighted the limitations of conventional time-frequency representations in modeling the complex doubly selective channels, particularly in high-mobility scenarios. To overcome these challenges, we emphasized the advantages of the delay-Doppler domain, where the inherent sparsity of such channels can be effectively leveraged for efficient signal processing.

To exploit this sparsity, we proposed a novel representation of the GFDM system in the delay-Doppler domain. By transforming the conventional time-frequency GFDM model, the system can better align with the characteristics of the channel, simplifying channel estimation and equalization. This transformation utilizes the symplectic finite Fourier transform (SFFT), delay-Doppler filtering, and the inverse discrete Zak transform (IDZT) to prepare the signal for transmission. This new GFDM system model forms the basis for advanced channel estimation techniques, which will be developed in the next chapter to address the challenges posed by doubly selective channels in high-mobility environments.

Chapter 3

Compressed Sensing Based Channel Estimation for GFDM systems in High Mobility Scenario

3.1 Introduction

In this chapter, we introduce a novel compressed sensing-based scheme for channel estimation designed for high-mobility scenarios. Unlike conventional methods that rely on dedicated pilot locations within the time-frequency domain, the proposed approach transforms the entire GFDM block into the delay-Doppler domain, where pilot and data symbols are superimposed. This eliminates the need for reserving specific frame locations for pilots, allowing the entire frame to be used for data transmission, thereby significantly enhancing spectral efficiency. To prevent interference between the superimposed pilot and data symbols, a data-dependent sequence, unknown to the receiver, is added to the original data in the time-frequency domain. This ensures separation of the pilot information from the data during the estimation process, without requiring guards between pilot and data symbols. At the receiver side, both channel estimation and data detection are performed directly in the delay-Doppler domain, by taking advantage of the sparsity of the channel in this representation. The proposed method is compared with conventional OFDM systems in terms

of mean squared error (MSE) and bit error rate (BER), demonstrating its superior performance in high-mobility scenarios.

3.2 Compressed Sensing

Compressed Sensing (CS) is an innovative technique in signal processing that enables the reconstruction of sparse signals from significantly fewer measurements than would be required under conventional Nyquist sampling [38], as shown in Fig. 3.1. This reduction in measurements is made possible by exploiting the intrinsic sparsity (or compressibility) of signals in a suitable transform domain. However, successful recovery critically depends on the sensing matrix, Φ , possessing certain favorable properties, such as low mutual coherence or satisfying the Restricted Isometry Property (RIP) [39]. Mutual coherence quantifies the maximum correlation between different columns of the sensing matrix, while RIP ensures that sparse vectors retain their distinct distance relationships once projected into the lower-dimensional measurement space. Specifically, the RIP provides a more generalized condition on a sensing (or measurement) matrix Φ . The matrix $\Phi \in \mathbb{C}^{M \times N}$ satisfies RIP of order K if there exists a constant $\delta_K \in (0, 1)$ such that for any K -sparse vector \mathbf{x} :

$$(1 - \delta_K) \|\mathbf{x}_s\|_2^2 \leq \|\Phi \mathbf{x}_s\|_2^2 \leq (1 + \delta_K) \|\mathbf{x}_s\|_2^2. \quad (14)$$

The Restricted Isometry Constant (RIC), δ_K , quantifies how well the sensing matrix preserves the Euclidean norm of any K -sparse vector. A smaller δ_K implies better preservation of distances, improving the performance of CS algorithms in accurately reconstructing sparse signals. However, no polynomial-time methods are known to determine whether a given sensing matrix satisfies the RIP. An alternative approach is to compute the mutual coherence of the sensing matrix.

The mutual coherence of a matrix, often denoted by $\mu(\Phi)$, measures the maximum correlation between any two distinct columns in the sensing matrix Φ . Formally, for columns ϕ_i and ϕ_j of Φ the mutual coherence is defined as the maximum normalized absolute inner product given by:

$$\mu(\Phi) = \max_{i \neq j} \frac{|\phi_i^H \phi_j|}{\|\phi_i\|_2 \|\phi_j\|_2}. \quad (15)$$

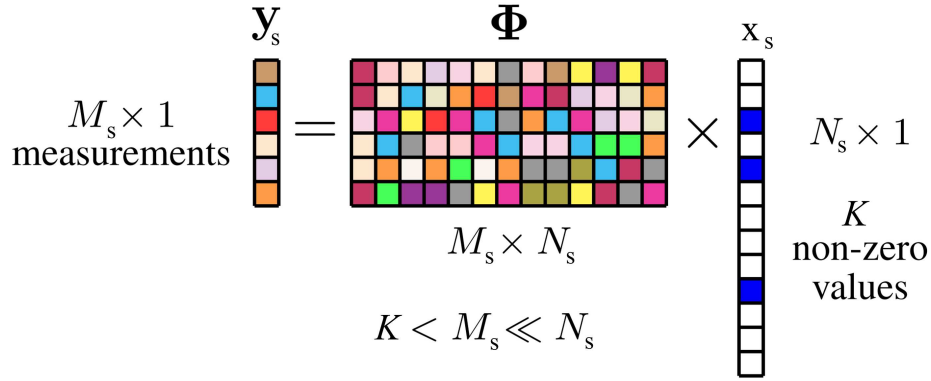


Figure 3.1: Illustration of a sparse signal \mathbf{x}_s and its measurement vector.

A lower mutual coherence indicates that the columns of Φ are less correlated, improving the conditions for accurately identifying the positions of the non-zero entries in a sparse signal.

3.2.1 Principles of Compressed Sensing

CS leverages the insight that if a signal is sparse or compressible in some domain, it can be reconstructed accurately using fewer samples than traditionally required, provided that the sensing matrix exhibits low mutual coherence or satisfies the RIP. The essence of CS lies in projecting the high-dimensional sparse signal onto a lower-dimensional measurement space, yet retaining enough information to enable accurate recovery. As illustrated in Fig. 3.1, the number of elements in the unknown vector \mathbf{x}_s can be greater than the number of measurements, but the signal remains recoverable due to its sparsity, i.e., only a relatively small number of non-zero elements. This characteristic is especially beneficial in scenarios where obtaining full measurements is impractical or resource-intensive. A variety of algorithms exist for sparse signal recovery under the CS framework [39], and they can be broadly categorized into two main groups:

- (1) **Convex Optimization Methods:** These methods, such as Basis Pursuit, formulate the recovery process as a convex minimization problem (e.g., ℓ_1 -norm minimization). Although they provide highly accurate recovery, their computational complexity can be prohibitive for real-time wireless communication systems [40].
- (2) **Greedy Algorithms:** Greedy algorithms have received considerable attention due to their

balance between computational efficiency and recovery performance. Orthogonal Matching Pursuit (OMP) [41] and Subspace Pursuit (SP) [42] are prominent examples. These algorithms iteratively refine estimates of the sparse signal by selecting columns of the sensing matrix most correlated with the current residual.

Among the greedy algorithms, SP has gained recognition for its robustness and computational efficiency. In each iteration, SP identifies a set of K columns (subspace) in the sensing matrix that exhibit the highest correlation with the measurement vector. The positions of the non-zero elements in the sparse signal are then located, and their magnitudes are updated using techniques such as least squares (LS) or minimum mean square error (MMSE) estimates. SP typically exhibits lower computational complexity than OMP for signals with a slow decay of non-zero elements, making it suitable for real-time communication systems. Another well-known greedy approach is Compressive Sampling Matching Pursuit (CoSaMP) [43]. While CoSaMP shares similarities with SP, it employs a slightly different strategy for selecting columns of the sensing matrix in each iteration. Though the two algorithms demonstrate comparable performance in many scenarios, SP often has a higher restricted isometry constant (RIC) threshold and enjoys well-characterized convergence properties. This makes SP a practical choice for real-time systems requiring reliable performance guarantees.

3.2.2 Subspace Pursuit (SP) Algorithm

Consider an unknown signal $\mathbf{x} \in \mathbb{R}^N$ and its measurement vector $\mathbf{y} \in \mathbb{R}^m$, linked by

$$\mathbf{y} = \Phi \mathbf{x}, \tag{16}$$

where $\Phi \in \mathbb{R}^{m \times N}$ is the sensing matrix. Define the support of a vector $\mathbf{x} = (x_1, \dots, x_N)$, denoted $\text{supp}(\mathbf{x})$, as the set of indices corresponding to its non-zero elements. The cardinality of the support, expressed by $\|\mathbf{x}\|_0$, is also known as the ℓ_0 norm, indicating the number of non-zero components in \mathbf{x} . The central challenge is to efficiently recover the sparse signal \mathbf{x} from the measurements \mathbf{y} . A

common starting point is to minimize the ℓ_0 norm,

$$\min \|\mathbf{x}\|_0 \quad \text{subject to} \quad \mathbf{y} = \Phi \mathbf{x}. \quad (17)$$

However, this ℓ_0 norm minimization is known to be NP-hard and thus impractical for real-world applications due to its high computational demand [44]. As a remedy, it is common to shift towards an ℓ_1 -minimization framework, a recognized simplification of the ℓ_0 problem:

$$\min \|\mathbf{x}\|_1 \quad \text{subject to} \quad \mathbf{y} = \Phi \mathbf{x}, \quad (18)$$

where $\|\mathbf{x}\|_1 = \sum_{i=1}^N |x_i|$ denotes the ℓ_1 norm. This relaxation is convex and can be solved using linear programming (LP) methods with computational complexity on the order of $O(m^2 N^{3/2})$ [45]. Despite the efficiency of ℓ_1 minimization, greedy algorithms such as the SP offer further computational advantages for certain types of sparse signals. It offers a balance between computational efficiency and reconstruction accuracy, making it well-suited for real-time communication systems. The SP algorithm specifically addresses cases where the sparsity level, denoted by K , is relatively low compared to the dimensions of the signal. In such cases, SP iteratively refines the support of the non-zero elements of \mathbf{x} , leading to efficient signal recovery under real-time constraints typical of communication systems.

The main steps of the SP algorithm are summarized in Algorithm 1. The goal is to recover the sparse signal $\mathbf{x} \in \mathbb{R}^N$ satisfying $\mathbf{y} = \Phi \mathbf{x} + \mathbf{e}$, where \mathbf{e} represents noise or modeling errors. In each iteration, a set of K columns of Φ is selected and refined to determine the support indices of the non-zero elements of \mathbf{x} .

To clarify the key steps in Algorithm 1, note that *projecting* a vector $\mathbf{y} \in \mathbb{R}^m$ onto the subspace spanned by the columns of $\Phi_I \in \mathbb{R}^{m \times |I|}$ (assuming $\Phi_I^* \Phi_I$ is invertible) results in:

$$\mathbf{y}_p = \Phi_I^\dagger \Phi_I^* \mathbf{y}, \quad \mathbf{y}_r = \mathbf{y} - \mathbf{y}_p, \quad (19)$$

where $\Phi_I^\dagger = (\Phi_I^* \Phi_I)^{-1} \Phi_I^*$ is the Moore-Penrose pseudoinverse of Φ_I . Moreover, $\Phi_{\mathcal{T}}$ is constructed from the columns of Φ indexed by the set \mathcal{T} . As mentioned before, the main difference

Algorithm 1 Subspace Pursuit Algorithm

- 1: **Input:** K, Φ, \mathbf{y}
 - 2: **Initialization:**
 - 3: $\mathcal{T}^0 \leftarrow K$ indices of the largest entries in $\Phi^H \mathbf{y}$.
 - 4: $\mathbf{y}_r^0 \leftarrow \text{resid}(\mathbf{y}, \Phi_{\mathcal{T}^0})$.
 - 5: **Iteration:** At the ℓ th iteration:
 - 6: $\tilde{\mathcal{T}}^\ell \leftarrow \mathcal{T}^{\ell-1} \cup \left\{ K \text{ indices of the largest entries in } \Phi^H \mathbf{y}_r^{\ell-1} \right\}$.
 - 7: $\mathbf{x}_p \leftarrow \Phi_{\tilde{\mathcal{T}}^\ell}^\dagger \mathbf{y}$.
 - 8: $\mathcal{T}^\ell \leftarrow \left\{ K \text{ indices of the largest entries of } \mathbf{x}_p \right\}$.
 - 9: $\mathbf{y}_r^\ell \leftarrow \text{resid}(\mathbf{y}, \Phi_{\mathcal{T}^\ell})$.
 - 10: **if** $\|\mathbf{y}_r^\ell\|_2 > \|\mathbf{y}_r^{\ell-1}\|_2$ **then** $\mathcal{T}^\ell \leftarrow \mathcal{T}^{\ell-1}$ **and stop.**
 - 11: **Output:**
 - 12: $\hat{\mathbf{x}}$ where $\hat{\mathbf{x}}_{\{1, \dots, N\} \setminus \mathcal{T}^\ell} = \mathbf{0}$ and $\hat{\mathbf{x}}_{\mathcal{T}^\ell} = \Phi_{\mathcal{T}^\ell}^\dagger \mathbf{y}$.
-

between OMP and SP is in the approach these two algorithms generate the set \mathcal{T} . OMP selects only one index during each iteration, and then this index remains in the set until the reconstruction process is finished. However, in the SP algorithm, the set \mathcal{T} is refined in each iteration. Hence, some indices denoted to be wrong can be removed from the list in later iterations. The authors in [42] show that the performance of reconstruction for the SP algorithm in terms of K outperforms the OMP algorithm, especially for higher K .

In greedy algorithms, the number of iterations directly affects computational cost. For OMP, each iteration selects one index, so finding all K indices requires K iterations, leading to $O(mNK)$ complexity, where m and N are the dimensions of the measurement vector and the original signal, respectively. However, [42] shows that in wireless communication systems with power-law decaying channel profiles, the number of iterations can often be upper-bounded by $O(mN \log(K))$. This is significantly more efficient than ℓ_1 -LP methods, which exhibit $O(m^2 N^{3/2})$ complexity. Consequently, SP is well-suited for large-scale and real-time applications, making it an attractive choice for channel estimation in high-mobility scenarios.

3.3 Proposed Channel Estimation using Subspace Pursuit

In communication systems, synchronization plays a crucial role in maintaining system performance, especially in high-mobility or multipath scenarios. Accurate timing synchronization is

essential to ensure that the receiver correctly identifies the beginning of each GFDM symbol block. Any timing offset can result in ISI and ICI, leading to significant degradation in performance. To focus exclusively on the evaluation of the proposed channel estimation methods, we assume perfect time synchronization at the receiver throughout this work.

In this section, we propose a new channel estimation method tailored for high-mobility scenarios using the Subspace Pursuit SP algorithm. We begin by revisiting the channel model in the delay-Doppler domain and then evaluate the transmitted signal as it propagates through this channel.

As noted earlier, the delay-Doppler domain provides a more compact representation of geometric channels compared to conventional time-delay or time-frequency domains, primarily due to the limited number of reflectors around the receiver. This sparsity is particularly useful for coping with rapidly time-varying channels. A generic LTV channel in the delay-Doppler domain can be modeled as [31]

$$h(\tau, \nu) = \sum_{i=1}^P h_i \delta(\tau - \tau_i) \delta(\nu - \nu_i), \quad (20)$$

where P is the number of dominant reflectors, h_i , τ_i and ν_i are the path gain, delay and Doppler shift of the i th path of the channel, respectively. Let Δf and T be the subcarrier spacing and symbol period, respectively. For notational purposes, we consider $\tau_i = \frac{l_i}{N\Delta f}$ and $\nu_i = \frac{k_i}{MT}$, where l_i and k_i are integers¹ and correspond to the delay and Doppler shift position in the delay-Doppler discrete grid. Further, $[0, \tau_{\max}]$ and $[-\nu_{\max}, \nu_{\max}]$ are assumed for the delay-Doppler domain channel $h(\tau, \nu)$, where τ_{\max} represents the maximum delay, and ν_{\max} represents the maximum Doppler offset. Therefore, consider l_{\max} and k_{\max} as the delay and Doppler taps corresponding to their respective maximum values. Note that $h(\tau, \nu)$ in (20) has a sparse representation, and thus, sparse recovery algorithms can be applied for channel estimation.

In our proposed method, we employ the new representation of the GFDM system in delay-Doppler domain, which is provided in section 2.3.2. Hence, the transmitted signal s in (13), is passed through a LTV channel which is modeled in (20). After sampling and discarding the CP in

¹The fractional delay and Doppler shift can be ignored if N and M are sufficiently large.

the time domain, the received signal can be written as [18]

$$r[q] = \sum_{i=1}^P h_i e^{j2\pi \frac{k_i(q-l_i)}{MN}} s[\langle q - l_i \rangle_{MN}] + v[q] \quad (21)$$

where $v[q]$ is the complex additive white Gaussian noise (AWGN) with variance σ^2 and $q = 0, \dots, MN - 1$. We rewrite (21) in the matrix form as

$$\mathbf{r} = \mathbf{H}\mathbf{s} + \mathbf{v}, \quad (22)$$

where $\mathbf{r} \in \mathbb{C}^{MN \times 1}$, $\mathbf{v} \sim \mathcal{CN}(0, \sigma^2 \mathbf{I}_{MN})$, and $\mathbf{H} \in \mathbb{C}^{MN \times MN}$ is the channel matrix defined as [18]

$$\mathbf{H} = \sum_{i=1}^P h'_i \mathbf{\Pi}^{l_i} \mathbf{\Delta}^{k_i}, \quad (23)$$

with $h'_i = h_i e^{-j2\pi \frac{k_i l_i}{MN}}$. Also, $\mathbf{\Pi} \in \mathbb{C}^{MN \times MN}$ denotes the permutation matrix used to model the delays as

$$\mathbf{\Pi} = \begin{bmatrix} 0 & 0 & \cdots & 0 & 1 \\ 1 & 0 & \cdots & 0 & 0 \\ 0 & 1 & \cdots & 0 & 0 \\ \vdots & \vdots & \ddots & \vdots & \vdots \\ 0 & 0 & \cdots & 1 & 0 \end{bmatrix}_{MN \times MN}$$

and $\mathbf{\Delta} \in \mathbb{C}^{MN \times MN}$ represents a diagonal matrix employed to model the Doppler shifts, which is defined as

$$\mathbf{\Delta} = \text{diag}[1, e^{\frac{j2\pi}{MN}}, \dots, e^{\frac{j2\pi(MN-1)}{MN}}]. \quad (24)$$

Each propagation path introduces an l_i -step cyclic shift of the transmitted signal vector \mathbf{s} , modeled by $\mathbf{\Pi}^{l_i}$, and modulates it with a carrier frequency k_i , represented by $\mathbf{\Delta}^{k_i}$.

To extract data symbols from (21), the channel coefficients require to be estimated and compensated. This would pose a challenge in the time-frequency domain since the channel changes rapidly during a GFDM symbol period in the time-varying channel. Hence, in the following, we develop an efficient estimation method in the delay-Doppler domain by using the sparsity properties of the

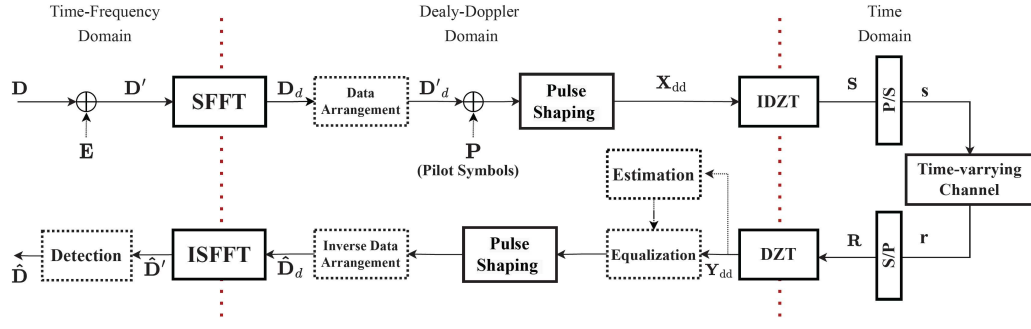


Figure 3.2: The block diagram of the new GFDM transceiver. All dotted blocks are associated with the channel estimation and data detection.

time varying channel model presented in (20). To improve the spectral efficiency of channel estimation, a superimposed scheme for pilot symbols and data is employed. In this approach, the entire frame initially consists solely of data symbols in the time-frequency domain. After transforming this frame into the delay-Doppler domain using SFFT, pilot symbols are superimposed onto specific locations of the newly transformed frame. This superposition involves adding pilot symbols to designated regions within the delay-Doppler grid while leaving the majority of the frame dedicated to data transmission. To address the interference caused by this superimposing, a data-dependent sequence \mathbf{E} is added to the original data \mathbf{D} to remove the impact of the data on the locations of the pilot symbols in the delay-Doppler domain, ensuring that the pilot symbols remain distinguishable during the channel estimation process, as shown in Fig. 3.2. Specifically, by distorting the data symbols in the time-frequency domain, their SFFT in the delay-Doppler domain at specific frequencies can be made identically zero. This ensures that designated regions in the delay-Doppler grid remain free of data interference, enabling pilot symbols to be clearly distinguishable for channel estimation. The energy of the distortion matrix \mathbf{E} should be minimized to avoid significant impact on the overall data transmission. For a fixed energy in \mathbf{D} , one effective solution for \mathbf{E} is to compute it as the cyclic mean of the data matrix \mathbf{D} , which ensures the desired zero values at specific frequencies. Mathematically, this is expressed as [47]

$$\mathbf{E} = -((1/Q)\mathbf{1}_Q \otimes \mathbf{I}_{N_r})\mathbf{D}, \quad (25)$$

where $Q = N/N_r$ is an integer number, $\mathbf{1}_Q$ is a vector of ones with length Q and \otimes represents the

Kronecker product. Also, $N_r = \lceil P_g/M \rceil$ is the minimum number of rows required to be zero in the matrix \mathbf{D}_d , where $P_g = N_P M_P$ and N_P and M_P are the pilot symbols along the delay and Doppler dimensions, respectively. In the delay-Doppler domain, arranging the data properly is critical to ensure that the pilot symbols can be added effectively without interfering with the data. Since the pilot symbols must occupy a dedicated frame in the middle of the delay-Doppler grid, it is necessary to manipulate the structure of the distorted data matrix \mathbf{D}_d . This manipulation ensures that specific regions in the grid are reserved for pilots while redistributing the displaced data to other parts of the frame. To achieve this, a data arrangement block is applied to \mathbf{D}_d . Hence, in the delay-Doppler domain, a data arrangement block is applied to the distorted data \mathbf{D}_d to place the N_r zero rows next to each other in the middle of the frame through a row switching operation on the obtained matrix as shown in Fig. 3.3. To obtain a $N_P \times M_P$ zero frame called pilot-guard frame in the middle of the $N \times M$ matrix \mathbf{D}'_d , the data symbols inside this frame are distributed to the zero symbols outside of this frame as shown in Fig. 3.3(b). Then, a known training matrix \mathbf{P} containing $N_P M_P$ pilot symbols is added to the distorted data to provide the input signal of the pulse shaping filter block (Fig. 3.4(a)). It is worth noting that based on the absolute value of the elements of matrix \mathbf{W} shown in Fig. 3.5, the lowest values are located in the middle of this matrix. Therefore, we place the pilot symbols in this area, and then adjust their power to achieve an accurate estimation.

As mentioned before, to exploit the sparsity properties of the channel in the delay-Doppler domain, estimation and equalization are performed in this domain. Using (13), we rewrite (22) in the delay-Doppler form as [18]

$$\begin{aligned}
\mathbf{y}_{\text{dd}} &= (\mathbf{F}_M \otimes \mathbf{I}_N) \mathbf{r} \\
&= (\mathbf{F}_M \otimes \mathbf{I}_N) \mathbf{H} (\mathbf{F}_M^H \otimes \mathbf{I}_N) \mathbf{x}_{\text{dd}} + (\mathbf{F}_M \otimes \mathbf{I}_N) \mathbf{v} \\
&= \tilde{\mathbf{H}} \mathbf{x}_{\text{dd}} + \mathbf{v}',
\end{aligned} \tag{26}$$

where \mathbf{y}_{dd} is the vectorized form of the matrix $\mathbf{Y}_{\text{dd}} = \mathbf{R} \mathbf{F}_M$ shown in Fig. 3.2. Furthermore, $\tilde{\mathbf{H}} = \text{circ}[\tilde{\mathbf{H}}_1, \dots, \tilde{\mathbf{H}}_{N-1}]$ is an $MN \times MN$ block-circulant matrix of the channel in the delay-Doppler domain, where $[\tilde{\mathbf{H}}_1, \dots, \tilde{\mathbf{H}}_{N-1}]$ are $M \times M$ circulant matrices [31]. Finally, it is easy to

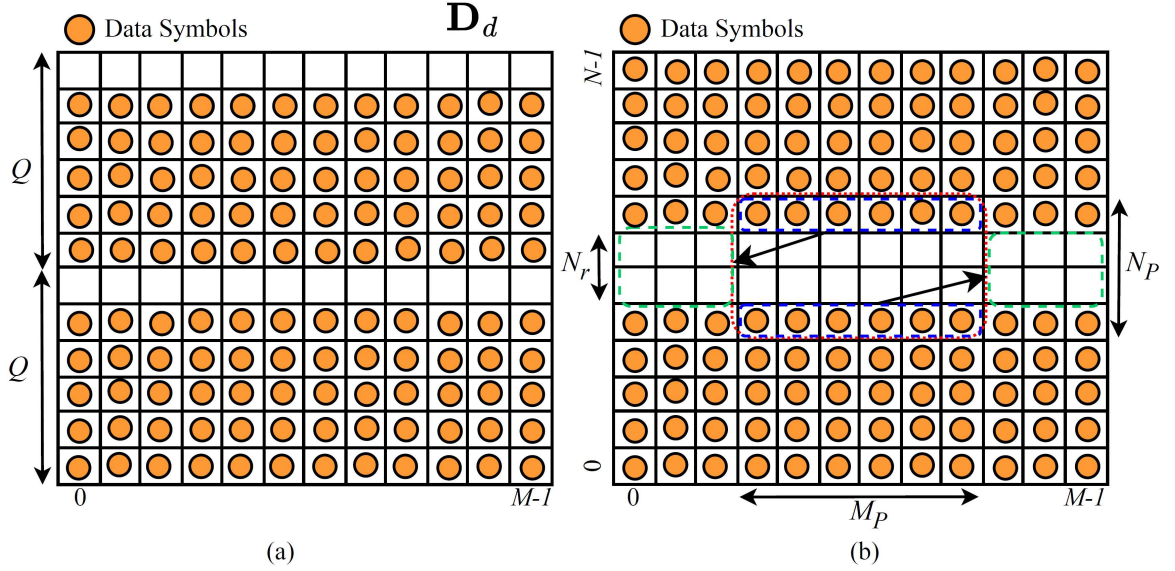


Figure 3.3: The discrete delay-Doppler grid for input and output matrix of data arrangement block. (a): The input of data arrangement block (i.e. the matrix \mathbf{D}_d). N_r zero rows are distributed with period of Q when \mathbf{E} is considered as (25). (b): Applying the row switching operation and distributing the data symbols inside the pilot-guard frame to the zeros symbols outside of this frame (Here, consider $N_r = 2$, $N_P = 4$ and $M_P = 6$ to explain further how this data spreading is performed.)

see that vector \mathbf{v}' has the same statistical properties as the noise in (22). Obtaining equation (26) for the channel estimation prior to applying the pulse shaping filter in the receiver prevents noise from being correlated.

For the channel estimation purpose, we rewrite (26) as a sparse signal recovery problem with the sensing matrix $\mathcal{A} = (\mathbf{X}_c \odot \mathbf{P}_{p,c})$ as

$$\mathbf{y}_{dd} = \mathcal{A}\mathbf{h} + \mathbf{v}', \quad (27)$$

where \mathbf{X}_c is an $MN \times MN$ block circulant matrix obtained in the same way as the matrix $\tilde{\mathbf{H}}$. Note that for non-ideal waveforms, $\tilde{\mathbf{H}}$ in (26) contains an extra phase factor in addition to the gain, delay and Doppler shift of each path (i.e. h'_i , τ_i and ν_i , respectively) [18]. We denote this factor as the $MN \times MN$ matrix

$$\mathbf{P}_{p,c}(a, b) = \begin{cases} \alpha_i(l, k), & l'_i \leq l < N \\ \alpha_i(l, k) \left(\frac{M-1}{M}\right) e^{-j2\pi \left(\frac{\leq k - k'_i > M}{M}\right)}, & 0 \leq l < l'_i \end{cases} \quad (28)$$

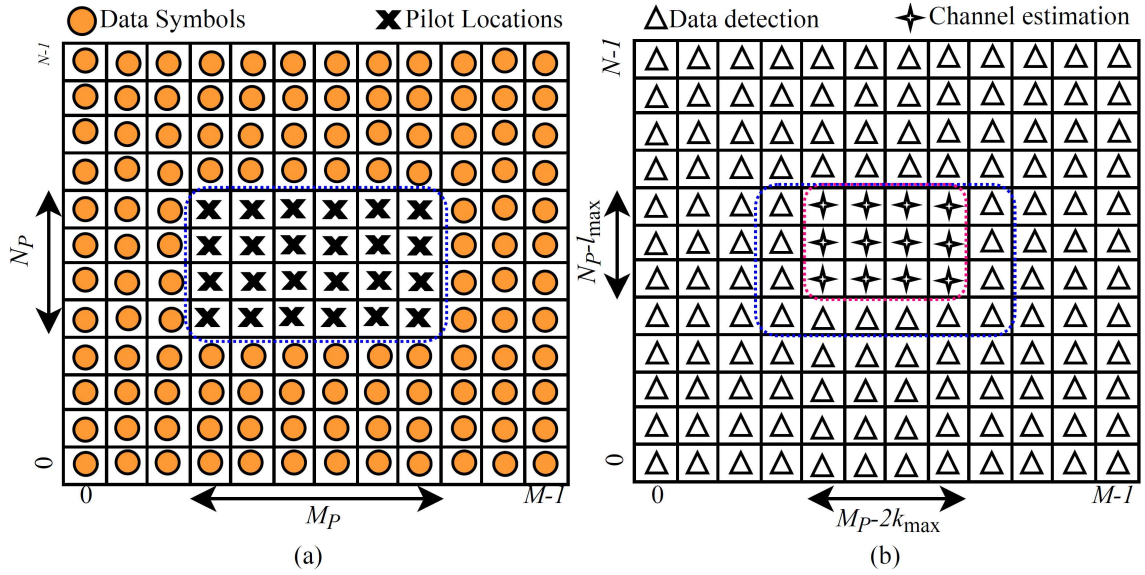


Figure 3.4: (a) The GFDM frame in the delay Doppler domain with pilots and guard intervals. (b) The symbols used in the channel estimation and data detection parts at the receiver side. Assume $l_{\max} = k_{\max} = 1$, $N_P = 4$ and $M_P = 6$.

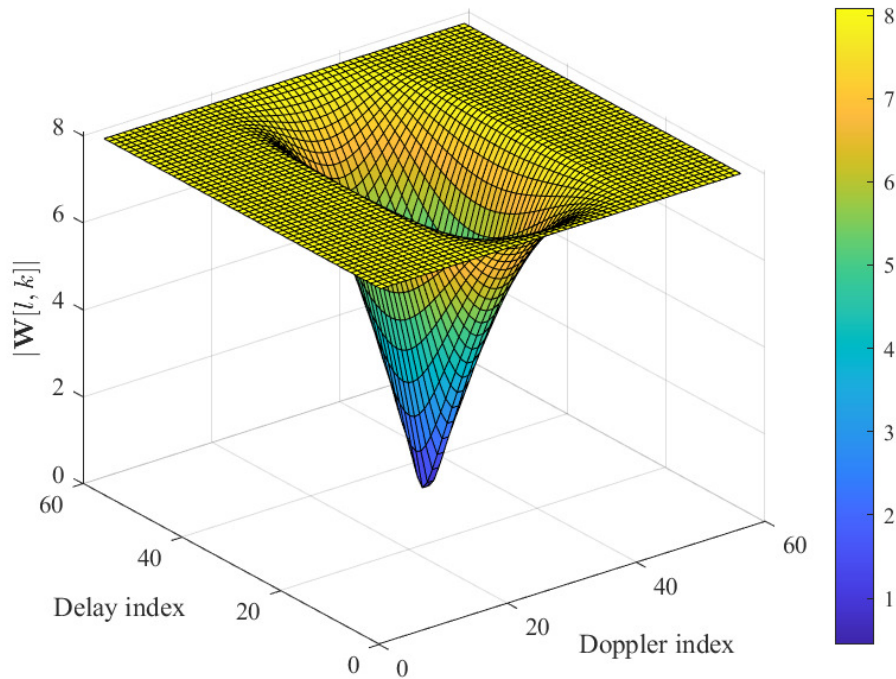


Figure 3.5: The absolute value of each element in the matrix \mathbf{W} (Raised cosine (RC) filter with a roll-off factor of 0.5) in the delay-Doppler domain, for $M = N = 57$.

where $\alpha_i(l, k) = e^{j2\pi(\frac{l-l'_i}{N})\frac{k'_i}{M}}$, $a = kN + l$ and $b = \langle k'_i \rangle_N \times N + l'_i$ with $l = 0, 1, \dots, N - 1$, $k = 0, 1, \dots, M - 1$, $l'_i = 0, 1, \dots, l_{\max}$ and $k'_i = -k_{\max}, \dots, 0, \dots, k_{\max}$. Also, the sparse vector \mathbf{h} is the first column of the matrix $\tilde{\mathbf{H}}$. For the channel estimation, we define $\mathbf{y}_{p,dd} \in \mathbb{C}^{(M_P - 2k_{\max})(N_P - l_{\max}) \times 1}$, whose elements are extracted from the vector \mathbf{y}_{dd} corresponding to the pilot part of the transmitted signal, specifically the symbols inside the red dotted-point box in Fig. 3.4(b). Additionally, the matrix \mathcal{A} will be updated to \mathcal{A}_p based on this modified vector $\mathbf{y}_{p,dd}$. Moreover, some indices in the vector \mathbf{h} are always zero due to the values of $l_{\max} < N$ and $k_{\max} < M$. Hence, only $(l_{\max} + 1)(2k_{\max} + 1)$ elements of \mathbf{h} are considered in the SP algorithm. Note that among these elements, only K_s elements are nonzero and should be estimated². In each iteration of the SP algorithm, a set of K_s columns of matrix \mathcal{A}_p is chosen, and then, by refining the set, the final list of the indices is obtained. Specifically, during each iteration, the algorithm selects iteratively a set of atoms that belongs to the subspace containing the largest energy of the sparse signal.

After channel estimation, to improve the detection performance, the impact of the pilot symbols on the data in the detection part needs to be removed. This task is accomplished by obtaining the new vector $\mathbf{y}'_{dd} = \mathbf{y}_{dd} - \hat{\mathbf{H}}\mathbf{p}$, where \mathbf{p} is the vectorized form of the pilot matrix \mathbf{P} , and $\hat{\mathbf{H}}$ is the estimated version of the matrix $\tilde{\mathbf{H}}$. Hence, the GFDM demodulator such as MMSE [46] is applied to the received signal \mathbf{y}'_{dd} for equalization purpose. Then, it is necessary to correct the phases introduced in (28) for the detection since they change based on different values of l and k in the matrix \mathbf{Y}_{dd} . Finally, it is essential to remove the contribution of the distortion matrix \mathbf{E} from the data before data detection. In the ideal scenario, i.e., when the channel estimation error and AWGN noise are absent, the output of the ISFFT block is equal to $\mathbf{D} - ((1/Q)\mathbf{1}_Q \otimes \mathbf{I}_{N_r})\mathbf{D}$. Note that $((1/Q)\mathbf{1}_Q \otimes \mathbf{I}_{N_r})\mathbf{D}$ is small compared to \mathbf{D} , and hence, it can be considered as extra additive noise. Therefore, an iterative scheme can be performed to detect the original data from the distorted data [47].

²For the distinct paths, K_s is considered the same as the number of channel path P .

Table 3.1: Simulation Parameters for SP-based Algorithm

Parameter	Value	Description
M	57	Number of subsymbols
N	57	Number of subcarriers
f_c	4 GHz	Carrier frequency
Δf	15 kHz	Subcarrier spacing
l_{\max}	4	Maximum delay
k_{\max}	4	Maximum Doppler (Speed: 300 kmph)
k_{\max}	3	Maximum Doppler (Speed: 150 kmph)
α_r	0.5	Roll-off factor (raised cosine filter)

3.4 Simulations

Simulation results for the proposed channel estimation method are presented in this section. The simulation parameters are presented in Table 3.1. As shown in this table, the number of subcarriers and subsymbols is 57 for each. Carrier frequency and subcarrier spacing are set to 4 GHz and 15 kHz, respectively. In this paper, a synthetic Rayleigh channel model is considered with a maximum delay of 4 and a Doppler shift of 4 or 3. Hence, a maximum Doppler speed of 300 kmph and 150 kmph can be assumed in this scenario. Finally, we employ an RC prototype filter with a roll-off factor of 0.5.

The mean squared error (MSE) of our proposed channel estimation method with different speeds is shown in Fig. 3.6. Note that the minimum-variance unbiased (MVU) estimator derived in the following serves as a benchmark since for linear equations it has the smallest variance among all unbiased estimators³ [48]. We use (27) to estimate the channel through MVU estimator. Using the components associated with the pilot-guard frame in the vector \mathbf{y}_{dd} , we can obtain the covariance matrix estimation as $\mathbf{C}_{\mathbf{h}} = \sigma^2(\mathcal{A}_p^H \mathcal{A}_p)^{-1}$. The figure illustrates how our proposed channel estimator outperforms the conventional MVU one by exploiting the sparsity properties of the channel. Specifically, for the same number of pilot symbols (i.e. $M_P = 15$ and $N_P = 10$), the MSEs of the proposed method with different speeds are close to one another, which indicates that our channel estimation method is not significantly sensitive to varying speeds. However, the MVU estimator

³For linear models, the MVU estimator attains the Cramér-Rao bound (CRB), meaning it has the lowest possible variance among all unbiased estimators [48].

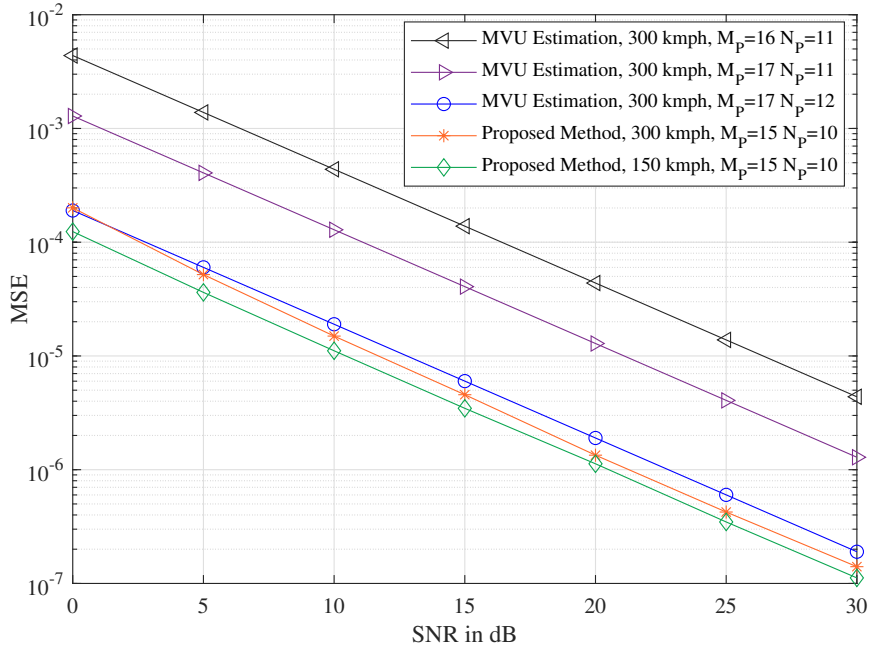


Figure 3.6: MSE performance comparison of the proposed method at different speeds versus MVU estimator.

cannot find the unique solution with this number of pilot symbols since the number of elements used for channel estimation in the measurement vector $\mathbf{y}_{p,dd}$ is less than the unknown elements of \mathbf{h} . On the other hand, only nonzero elements of the channel vector \mathbf{h} , which is less than the size of the measurement vector, are estimated in our method. Note that to achieve better results for the MVU estimator, more pilot symbols will be required to assist in the channel estimation, as shown in this figure. Hence, the MVU estimator can reach our proposed method at the cost of pilot overhead.

Fig. 3.7 is provided to support the discussion on the MVU estimator's dependence on pilot symbols. In other words, for a range of pilot numbers, the proposed method achieves lower MSE compared to the unbiased estimators, highlighting the advantages of compressed sensing-based approaches. According to this figure, MSE is shown as a function of the number of pilot symbols⁴. The purpose of this figure is to highlight the trade-off between pilot overhead and estimation accuracy, showing that while the MVU estimator can approach the performance of our proposed method, it requires a significantly higher number of pilot symbols. The figure starts at $M_p = N_p = 9$ because

⁴Note that we consider the same values for both M_p and N_p in our comparison

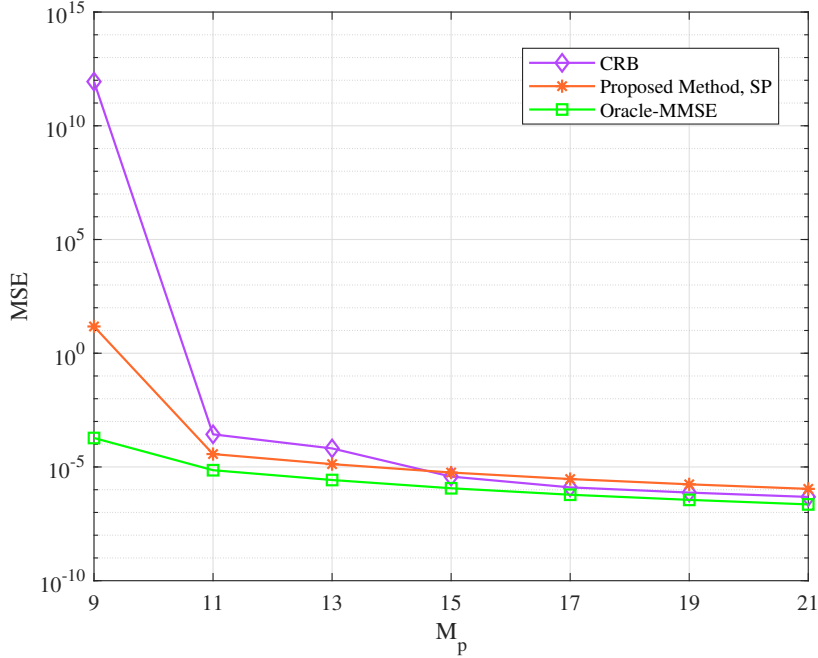


Figure 3.7: MSE performance comparison among the proposed SP-based channel estimator and the theoretical benchmarks (CRB and Oracle-MMSE) at an SNR of 10 dB, where $M_p = N_p$ and $k_{\max} = l_{\max}$.

we consider two different groups of pilot allocations. The first group corresponds to the minimum number of pilots required in a compressed sensing-based approach, such as the SP method. This number is derived based on the theoretical bound $O(cK_s \log(N_s/K_s))$, where c is a small constant (around 0.28 in many scenarios [49]), K_s is the sparsity level (number of nonzero elements in the channel), and N_s is the total length of the unknown channel vector h . The second group of pilot allocations corresponds to a superimposed-pilot-data transmission scheme, where both pilot and data symbols are sent in the same frame. To ensure proper separation between the pilot and data regions, a guard interval, which is associated with the maximum delay and Doppler, is typically introduced. Instead of leaving this guard interval empty (zero values), additional pilot symbols are inserted, leading to improved channel estimation accuracy. In this figure, CRB is used as the benchmark for unbiased estimators, while the Oracle-MMSE serves as a benchmark for biased estimators such as the SP algorithm. The Oracle-MMSE estimator, which assumes perfect knowledge of the delay-Doppler domain channel, is given by $\hat{\mathbf{h}}_{\text{O-MMSE}} = (\frac{1}{\sigma^2}) (\frac{1}{\sigma^2} \mathcal{A}_0^H \mathcal{A}_0 + \mathbf{I}_{K_s})^{-1} \mathcal{A}_0^H \mathbf{y}_{\text{p,dd}}$ [50].

In Fig. 3.8, we investigate the bit error rate (BER) performance of the proposed method in the

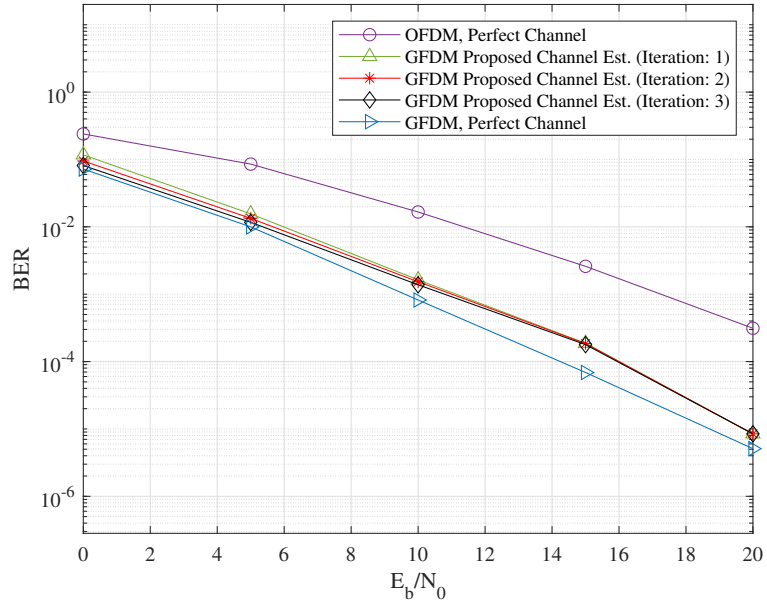


Figure 3.8: BER performance comparison of the proposed method versus perfect knowledge of the channel available at the receiver side.

presence of a time-variant channel. The BER results are based on a 4-QAM modulation scheme with convolution coding and the code rate of 1/2. The BER performance with perfect channel is provided when the receiver has perfect knowledge of the channel information. As shown in this figure, the BER performance of the GFDM system is superior to that of the OFDM system. This is due to the poor performance of OFDM systems in the time-varying channel. Furthermore, we employ the iterative detector to cope with the added distortion matrix \mathbf{E} . As shown in this figure, for higher SNR values, the BER of our proposed method using one iteration in the detector coincides with that of the proposed method using a higher number of iterations. Also, at higher SNRs, the BER of our proposed method approaches that of the GFDM system with perfect channels.

3.5 Conclusion

In this chapter, we introduced a novel method for channel estimation in GFDM systems using the Subspace Pursuit (SP) algorithm, specifically designed for high-mobility scenarios. By leveraging the inherent sparsity of channels in the delay-Doppler domain, we transformed the conventional

GFDM system model into this domain to enhance estimation accuracy and computational efficiency. We proposed a unique approach of embedding pilot symbols directly within the delay-Doppler domain, eliminating the need for dedicated pilot regions in the time-frequency domain. Additionally, a data-dependent sequence was superimposed onto the original data in the time-frequency domain to mitigate interference with pilot symbols, ensuring reliable channel estimation while maximizing spectral efficiency. The effectiveness of this superimposed technique not only simplifies the channel estimation process but also significantly improves the spectral efficiency compared to conventional methods. Simulation results demonstrate that the proposed method not only enhances channel estimation accuracy but also achieves superior performance compared to traditional OFDM systems, even when the latter have perfect channel state information at the receiver. These advancements pave the way for more efficient and robust communication in rapidly changing wireless environments, highlighting the potential of delay-Doppler domain-based approaches in future wireless communication systems.

Chapter 4

Sparse Bayesian Learning Channel

Estimation in RIS-aided GFDM Systems

4.1 Introduction

The integration of RIS with GFDM systems represents a promising new direction in wireless communications, offering the potential for enhanced spectral efficiency, improved coverage, and greater energy savings. By adaptively controlling the reflection coefficients of an RIS, the propagation environment can be dynamically reshaped, leading to more favorable channel conditions. Fig. 4.1 illustrates several key functionalities of RIS in wireless communication systems. Firstly, RIS can be employed for coverage extension, as shown in part (a) of the figure. In scenarios where direct line-of-sight (LoS) communication is obstructed, RIS creates a virtual LoS link by reflecting the signal, effectively overcoming coverage challenges. Additionally, as demonstrated in part (b), RIS improves the channel rank condition by transforming low-rank channels into high-rank ones through intelligent signal redirection, thereby enabling enhanced spatial multiplexing and data throughput. Furthermore, part (c) highlights the capability of RIS to refine channel statistics by mitigating fast Rayleigh fading and introducing slow or Rician fading characteristics, resulting in more stable and reliable communication links. Finally, part (d) showcases the role of RIS in interference suppression, where it redirects interfering signals away from desired receivers, ensuring improved signal quality and a higher quality of service [51]. These diverse capabilities make RIS a transformative

technology for modern wireless communication systems. However, realizing its full potential requires precise channel estimation, which becomes increasingly challenging in RIS-aided systems due to the high dimensionality of the resulting channel matrices. Conventional channel estimation methods often fall short in effectively addressing these challenges. Sparse Bayesian Learning (SBL) has recently emerged as a particularly powerful method for channel estimation in scenarios characterized by both high dimensionality and sparsity. Unlike traditional compressed sensing techniques—and especially compared to greedy algorithms such as SP, which typically require prior knowledge of the sparsity level and are highly sensitive to the choice of sensing matrix and stopping threshold—SBL employs a data-driven approach to infer the optimal sparsity structure. Its automatic relevance determination mechanism effectively mitigates the risk of error propagation that can occur when greedy methods make an early incorrect atom selection. In other words, SBL does not require a priori knowledge of the sparsity level, resulting in improved estimation accuracy and resolution. By adaptively tuning its hyperparameters to match varying channel conditions, SBL often outperforms conventional compressed sensing methods, making it a flexible and reliable solution for modern wireless systems. However, while SBL’s excellent reconstruction accuracy and robustness are key advantages, these benefits come at the cost of increased computational complexity compared to greedy approaches.

In this chapter, we propose and investigate an SBL-based channel estimation strategy in RIS-aided GFDM systems. Our novel framework leverages the inherent strengths of SBL and the reconfigurability of RIS to address the fundamental challenges of next-generation wireless networks. By doing so, we aim to demonstrate that SBL provides a superior alternative to conventional methods, achieving higher accuracy, more efficient resource allocation, and greater reliability.

4.2 RIS-aided System Model

An RIS-aided GFDM system is depicted in Fig. 4.2, where a single-antenna base station (BS) communicates with a single-antenna user moving at high speed. The RIS, placed to enhance the link between the user and the BS, consists of N_{RIS} passive reflecting elements. Although a large number of RIS elements improves signal reflection power, it also increases overhead and complexity in

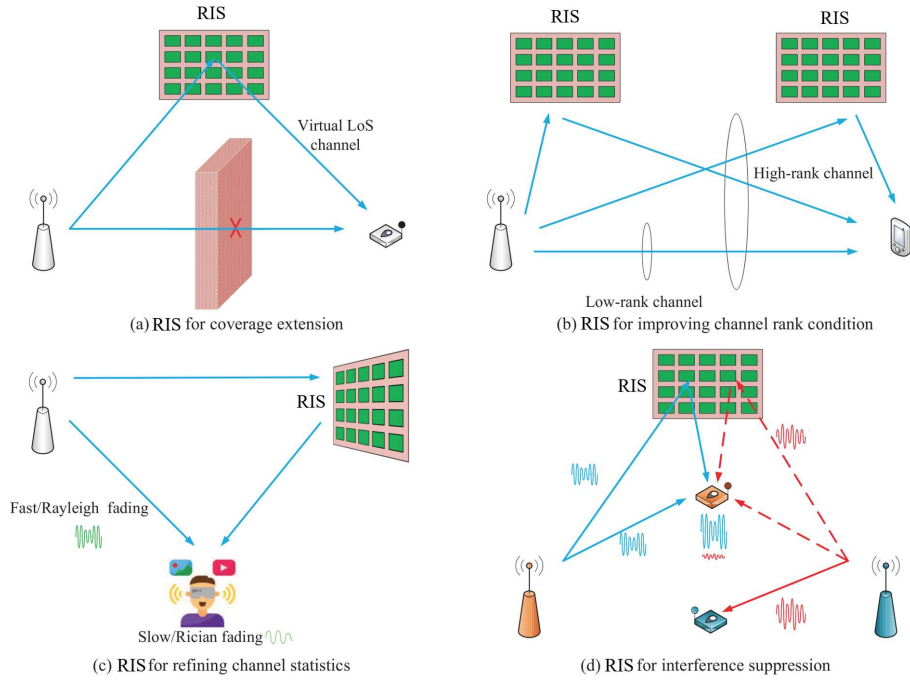


Figure 4.1: Primary functions of RIS in wireless channel reconfiguration [51].

channel estimation and reflection optimization. Each RIS element is controlled by a smart controller that dynamically adjusts its reflection coefficients.

Recall from (20) in the previous chapter that a general LTV channel in the delay-Doppler domain can be expressed as:

$$h(\tau, \nu) = \sum_{p=1}^P h_p \delta(\tau - \tau_p) \delta(\nu - \nu_p).$$

In the RIS-assisted scenario, we identify three main channels:

- (1) *Direct channel* between the user and BS:

$$h_d(\tau_d, \nu_d) = \sum_{p=1}^{P_d} h_{d,p} \delta(\tau_d - \tau_{d,p}) \delta(\nu_d - \nu_{d,p}),$$

- (2) *User-to-RIS channel*:

$$h_g(\tau_g, \nu_g) = \sum_{p=1}^{P_g} h_{g,p} \delta(\tau_g - \tau_{g,p}) \delta(\nu_g - \nu_{g,p}),$$

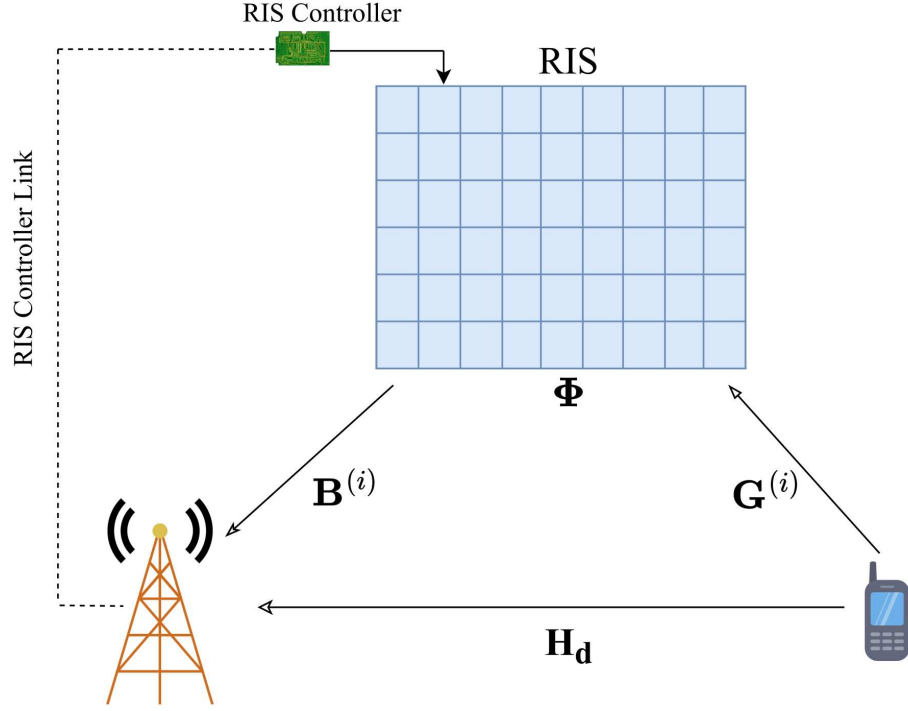


Figure 4.2: RIS-assisted GFDM system with a single-antenna user and BS.

(3) *RIS-to-BS channel:*

$$h_b(\tau_b, \nu_b) = \sum_{p=1}^{P_b} h_{b,p} \delta(\tau_b - \tau_{b,p}) \delta(\nu_b - \nu_{b,p}),$$

where P_d , P_g , and P_b denote the dominant path counts of the direct link, the user-RIS link, and the RIS-BS link, respectively. The notation $\tau_{\cdot,p}$ and $\nu_{\cdot,p}$ represent the delay and Doppler shift of the p th path in each channel.

To derive the time-domain input-output relationship for an RIS-aided system, consider first the signal contributed by the i th RIS element. Let $\mathbf{r}^{(i)} \in \mathbb{C}^{MN \times 1}$ be the received signal due to the user-RIS-BS path through element i , modeled as

$$\mathbf{r}^{(i)} = \phi^{(i)} \mathbf{B}^{(i)} \mathbf{G}^{(i)} \mathbf{s}, \quad (29)$$

where $\phi^{(i)} = \varphi_i e^{j\theta_i}$ is the reflection coefficient of the i th RIS element, with amplitude φ_i and phase shift θ_i . $\mathbf{G}^{(i)}, \mathbf{B}^{(i)} \in \mathbb{C}^{MN \times MN}$ denote the time-domain channel from the user to the i th RIS element, and from the i th RIS element to the BS, respectively. Following the channel matrix

introduced in (23), each channel matrix $\mathbf{G}^{(i)}$ and $\mathbf{B}^{(i)}$ can be expressed in terms of delay and Doppler shifts:

$$\mathbf{G}^{(i)} = \sum_{\alpha=1}^{P_g} g_{\alpha}^{(i)} \mathbf{\Pi}^{l_{\alpha}^{(i)}} \mathbf{\Delta}^{k_{\alpha}^{(i)}}, \quad \mathbf{B}^{(i)} = \sum_{\beta=1}^{P_b} h_{\beta}^{(i)} \mathbf{\Pi}^{l_{\beta}^{(i)}} \mathbf{\Delta}^{k_{\beta}^{(i)}}, \quad (30)$$

where

$$g_{\alpha}^{(i)} = g_{\alpha}^{(i)} \exp\left(-j \frac{2\pi k_{\alpha} l_{\alpha}}{MN}\right), \quad h_{\beta}^{(i)} = h_{\beta}^{(i)} \exp\left(-j \frac{2\pi k_{\beta} l_{\beta}}{MN}\right),$$

and $\mathbf{\Pi}$, $\mathbf{\Delta}$ are the permutation (cyclic shift) and Doppler diagonal matrices, respectively, as defined in (23). The end-to-end input-output relationship in the presence of noise in the time domain can be obtained by summing the received signals from all RIS elements as

$$\begin{aligned} \mathbf{r} &= \left(\mathbf{H}_d + \sum_{i=1}^{N_{\text{RIS}}} \phi^{(i)} \mathbf{B}^{(i)} \mathbf{G}^{(i)} \right) \mathbf{s} + \mathbf{v} \\ &= (\mathbf{H}_d + \mathbf{H}_{\text{ris}} \mathbf{\Phi}) \mathbf{s} + \mathbf{v} \\ &= \bar{\mathbf{H}} \mathbf{s} + \mathbf{v}, \end{aligned} \quad (31)$$

where $\mathbf{H}_{\text{ris}} = [(\mathbf{H}_{\text{ris}}^{(1)}), (\mathbf{H}_{\text{ris}}^{(2)}), \dots, (\mathbf{H}_{\text{ris}}^{(N_{\text{RIS}})})]$ is the cascade channel with $\mathbf{H}_{\text{ris}}^{(i)} = \mathbf{B}^{(i)} \mathbf{G}^{(i)}$. Also, $\mathbf{\Phi} \in \mathbb{C}^{N_{\text{RIS}} MN \times MN}$ is a matrix comprising the reflection coefficients of N_{RIS} elements. Specifically, we have

$$\mathbf{\Phi} = \left[\varphi_1 e^{j\theta_1}, \varphi_2 e^{j\theta_2}, \dots, \varphi_{N_{\text{RIS}}} e^{j\theta_{N_{\text{RIS}}}} \right]^T \otimes \mathbf{I}_{MN},$$

where \otimes denotes the Kronecker product and each diagonal entry corresponds to a reflection element at the RIS. By manipulating the reflection coefficients $\phi^{(i)} = \varphi_i e^{j\theta_i}$, one can dynamically shape the propagation environment to improve link quality, even in high-mobility scenarios. However, as N_{RIS} increases, accurate channel estimation and efficient reflection design become more challenging. The following section explores these challenges and introduces advanced estimation techniques and low-complexity reflection optimization to manage the RIS-aided system's complexity.

4.3 Proposed Channel Estimation with Sparse Bayesian Learning

In this section, we introduce a novel channel estimation framework based on SBL for RIS-aided GFDM systems. The inherent sparsity of the channel in the delay-Doppler domain, especially in high-mobility environments, is exploited to obtain accurate estimates of the cascaded channels. This precise estimation is essential not only for reliable data detection in GFDM but also for optimizing the reflection coefficients of the RIS. Our proposed method is executed in two distinct phases [24]. In the first phase, a pre-designed reflection coefficient pattern is employed to estimate the effective channel $\bar{\mathbf{H}}$ in (31). This pre-designed reflection coefficient pattern enables us to isolate and exploit the cascaded channel associated with each RIS element, thereby facilitating robust channel estimation via SBL. In the second phase, these estimated channels are used to optimize the reflection coefficients represented by the matrix Φ . The phase optimization aims to align the reflected signals constructively at the receiver, thereby enhancing the overall system performance. The detailed discussion of both channel estimation and reflection coefficient optimization follows in the subsequent subsections.

4.3.1 Channel Estimation Algorithm

We begin by considering the overall effective channel in the system, denoted as $\bar{\mathbf{H}}$ in (31), which integrates both the direct channel and the cascaded channels via the RIS. In our framework, as mentioned before, not only must the channel coefficients be estimated, but the reflection coefficients Φ of the RIS also need to be determined. To this end, our transmission protocol divides each GFDM frame into two sub-frames, as illustrated in Fig. 4.3(a). The initial sub-frame consists of $(N_{\text{RIS}} + 1)$ consecutive pilot symbols, while the remaining sub-frame carries pure data symbols. By using this protocol, we first estimate the entire effective channel $\bar{\mathbf{H}}$ from the received pilot signals.

Once the effective channel is estimated, we can further decompose it to extract the individual cascaded channels corresponding to each RIS element. This is achieved by transmitting the set of $(N_{\text{RIS}} + 1)$ GFDM pilot symbols, which enables us to reversely isolate the cascade channels associated with each RIS element. The superimposed pilot scheme discussed in Section 3 is applied here to enhance spectral efficiency—pilot symbols are embedded within the data, and a pilot-guard

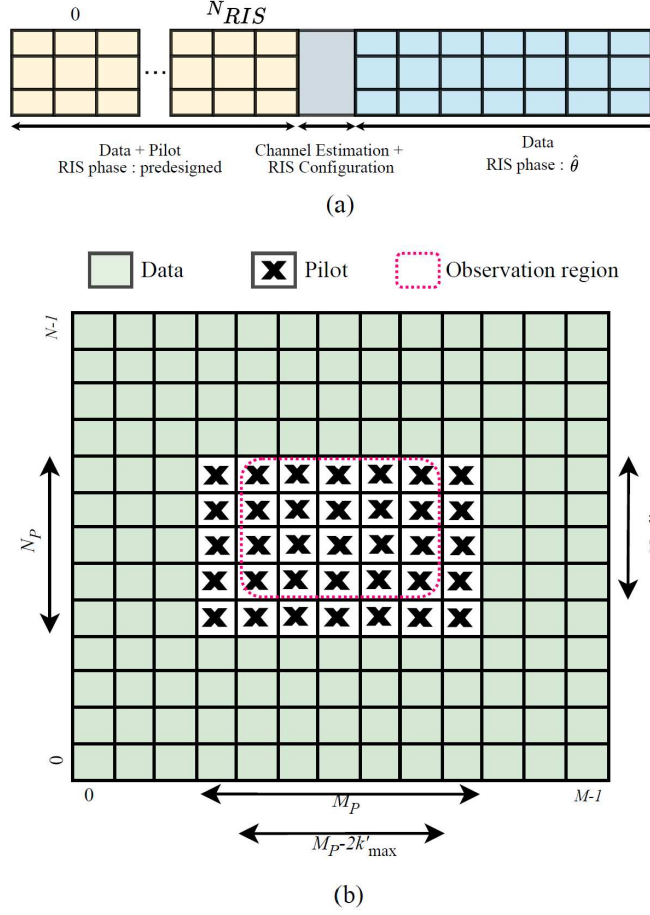


Figure 4.3: The transmission protocol; (a) $N_{RIS} + 1$ pilot symbols for the training phase followed by pure data symbols. (b) One of the pilot symbols considered in the training phrase. Assume $l'_{\max} = k'_{\max} = 1$, $N_P = 5$ and $M_P = 7$.

frame in the delay-Doppler domain is formed by removing the data interference at the designated pilot locations (see Fig. 4.3(b)).

In the delay-Doppler domain, the received signal through the effective channel is given by

$$\begin{aligned}
\mathbf{y}_{dd} &= (\mathbf{F}_M \otimes \mathbf{I}_N) \mathbf{r} \\
&= (\mathbf{F}_M \otimes \mathbf{I}_N) \tilde{\mathbf{H}} (\mathbf{F}_M^H \otimes \mathbf{I}_N) \mathbf{x}_{dd} + (\mathbf{F}_M \otimes \mathbf{I}_N) \mathbf{v} \\
&= \tilde{\mathbf{H}}_{\text{eff}} \mathbf{x}_{dd} + \mathbf{v}',
\end{aligned} \tag{32}$$

where $\tilde{\mathbf{H}}_{\text{eff}} = \tilde{\mathbf{H}}_d + \tilde{\mathbf{H}}_{\text{ris}} \Phi$, with $\tilde{\mathbf{H}}_d$ and $\tilde{\mathbf{H}}_{\text{ris}}$ representing the direct channel and the cascaded channels in the delay-Doppler domain, respectively. The first column of $\tilde{\mathbf{H}}_{\text{eff}}$ contains \check{P} non-zero

elements, where $P_d \leq \check{P} \leq P_d + N_{\text{RIS}}P_gP_b$. Since $\check{P} \ll MN$, we can formulate the estimation of the effective channel as a sparse signal recovery problem:

$$\mathbf{y}_{\text{dd}} = \mathcal{A}\mathbf{h} + \mathbf{v}', \quad (33)$$

where the sparse vector \mathbf{h} is the first column of $\tilde{\mathbf{H}}_{\text{eff}}$, and the sensing matrix $\mathcal{A} = (\mathbf{X}_c \odot \mathbf{P}_{p,c})$ has been detailed in Chapter 3. Note that the effective channel matrix $\tilde{\mathbf{H}}_{\text{eff}}$ maintains the block-circulant structure of the system, and hence we can employ the sparse recovery algorithms for channel estimation. Furthermore, during the estimation stage, we focus solely on the entries of \mathbf{y}_{dd} corresponding to the pilot region (indicated by the red dotted box in Fig. 4.3(b)).

Having formulated the sparse recovery problem in (33), we now focus on SBL, a probabilistic framework that leverages the channel's inherent sparsity for improved estimation performance. By integrating prior knowledge about the channel's sparse structure into the Bayesian inference process, SBL is capable of not only accurately estimating the key channel parameters but also identifying the most likely locations of the non-zero elements in the sparse representation.

In the SBL framework for channel estimation, the noise term \mathbf{v}' in (33) is modeled as Gaussian white noise with zero mean and a precision α_0 (i.e., the reciprocal of the variance). Its probability density function is given by

$$p(\mathbf{v}' | \alpha_0) = \mathcal{N}(\mathbf{v}' | 0, \alpha_0^{-1}\mathbf{I}), \quad (34)$$

where \mathbf{I} is the identity matrix. We further assume that α_0 follows a Gamma distribution parameterized by the hyperparameters a and b :

$$p(\alpha_0; a, b) = \Gamma(\alpha_0 | a, b). \quad (35)$$

This modeling framework enables us to express the likelihood function of the received signal \mathbf{y}_{dd} as

$$p(\mathbf{y}_{\text{dd}} | \mathcal{A}, \mathbf{h}, \alpha_0) = \mathcal{N}(\mathbf{y}_{\text{dd}} | \mathcal{A}\mathbf{h}, \alpha_0^{-1}\mathbf{I}). \quad (36)$$

Within the SBL framework, the sparse channel vector \mathbf{h} is modeled by a Gaussian distribution with zero mean and a diagonal covariance matrix $\mathbf{\Lambda}$, where $\mathbf{\Lambda} = \text{diag}(\boldsymbol{\alpha})$ and $\boldsymbol{\alpha}$ comprises individual

precision parameters:

$$p(\mathbf{h} \mid \boldsymbol{\alpha}) = \mathcal{N}(\mathbf{h} \mid \mathbf{0}, \boldsymbol{\Lambda}). \quad (37)$$

Each component α_i of $\boldsymbol{\alpha}$ is assumed to follow an independent Gamma distribution:

$$p(\alpha_i; \lambda) = \Gamma\left(\alpha_i \mid 1, \frac{\lambda}{2}\right), \quad i = 1, \dots, L, \quad (38)$$

where L is the number of elements in \mathbf{h} . Moreover, to further promote sparsity, a Laplace prior may be applied to each element h_i of \mathbf{h} :

$$p(h_i \mid \lambda) = \text{Laplace}\left(0, \frac{1}{\sqrt{\lambda}}\right), \quad i = 1, \dots, L. \quad (39)$$

Combining these elements, the joint probability density function of the model is

$$p(\mathbf{y}_{\text{dd}}, \mathbf{h}, \boldsymbol{\alpha}, \alpha_0) = p(\mathbf{y}_{\text{dd}} \mid \mathbf{h}, \alpha_0) p(\mathbf{h} \mid \boldsymbol{\alpha}) p(\boldsymbol{\alpha}) p(\alpha_0). \quad (40)$$

The posterior probability of \mathbf{h} given the observed data \mathbf{y}_{dd} is then derived as a Gaussian distribution [54]:

$$p(\mathbf{h} \mid \mathbf{y}_{\text{dd}}, \boldsymbol{\alpha}, \alpha_0) = \mathcal{N}(\mathbf{h} \mid \boldsymbol{\mu}, \boldsymbol{\Sigma}), \quad (41)$$

with mean $\boldsymbol{\mu}$ and covariance $\boldsymbol{\Sigma}$ defined by $\boldsymbol{\mu} = \alpha_0 \boldsymbol{\Sigma} \mathcal{A}^T \mathbf{y}_{\text{dd}}$, $\boldsymbol{\Sigma} = \left(\alpha_0 \mathcal{A}^T \mathcal{A} + \boldsymbol{\Lambda}^{-1}\right)^{-1}$. To estimate the hyperparameters $\boldsymbol{\alpha}$ and α_0 , we employ the Expectation-Maximization (EM) algorithm [55]. The hyperparameters are iteratively updated by maximizing the expected log-likelihood:

$$(\boldsymbol{\alpha}^{\text{new}}, \alpha_0^{\text{new}}) = \arg \max_{\boldsymbol{\alpha}, \alpha_0} \mathbb{E} \left[\ln p(\mathbf{y}_{\text{dd}}, \mathbf{h}, \boldsymbol{\alpha}, \alpha_0) \right]. \quad (42)$$

The iterative updates for the hyperparameters are given by [56]:

$$\alpha_i^{\text{new}} = \frac{\sqrt{1 + 4\lambda (\Sigma_{ii} + \mu_i^2)} - 1}{2\lambda}, \quad i = 1, \dots, L, \quad (43)$$

$$\alpha_0^{\text{new}} = \frac{2a - 2 + P_Y}{2b + \mathbb{E} [\|\mathbf{y}_{\text{dd}} - \mathcal{A} \mathbf{h}\|_2^2]}, \quad (44)$$

where $P_y = (M_p - 2K'_{\max}) \times (N_p - l'_{\max})$ is the number of received channel estimation symbols, and the expectation is given by

$$\mathbb{E} [\|\mathbf{y}_{\text{dd}} - \mathcal{A}\mathbf{h}\|_2^2] = \alpha_0^{-1} \sum_{i=1}^L (1 - \alpha_i \Sigma_{ii}) + \|\mathbf{y}_{\text{dd}} - \mathcal{A}\boldsymbol{\mu}\|_2^2. \quad (45)$$

These updates form part of an iterative process to maximize the expected log-likelihood, thereby refining the estimates of the sparse channel \mathbf{h} and its associated hyperparameters. The complete procedure for SBL-based channel estimation is summarized in Algorithm 2. Note that in step 7 of this algorithm, there are two conditions for terminating the iteration. If either condition is satisfied, the iteration process is stopped. The first condition is given by $\frac{\|\boldsymbol{\alpha}^{\text{new}} - \boldsymbol{\alpha}\|_2^2}{\|\boldsymbol{\alpha}\|_2^2} < 10^{-5}$, while the second condition is reaching the predefined maximum number of iterations (e.g., 150 in many cases). Moreover, the SBL algorithm has been proved to converge in various scenarios [57].

Algorithm 2 Sparse Bayesian Learning-Based Channel Estimation Algorithm

- 1: **Initialize:** Set initial values for α_0 , $\boldsymbol{\alpha}$, and hyperparameters a , b ; set iteration counter $j = 0$.
 - 2: **Input:** \mathbf{y}_{dd} , \mathcal{A} , P_y , L
 - 3: **repeat**
 - 4: Compute $\boldsymbol{\mu}$ and $\boldsymbol{\Sigma}$ using the current α_0 and $\boldsymbol{\alpha}$
 - 5: Update $\boldsymbol{\alpha}$ and α_0 using (43) and (44)
 - 6: Set $j = j + 1$
 - 7: **until** a stopping criterion is met
 - 8: **Output:** $\hat{\mathbf{h}} = \boldsymbol{\mu}$
-

Ultimately, through this estimation process we obtain the effective channel matrix, $\tilde{\mathbf{H}}_{\text{eff}}$, which encompasses both the cascaded channel via the RIS and the direct channel between the user and the BS. By transmitting $N_{\text{RIS}} + 1$ GFDM pilot symbols, we can reliably extract these channel components. These channel estimates form the basis for the subsequent RIS phase optimization, which will be discussed in the next subsection.

Note that, in terms of computational complexity, the SBL algorithm has a complexity of $\mathcal{O}(J \times K_s L^2)$, where K_s and L represent the number of nonzero elements and the total length of the channel vector \mathbf{h} , respectively, and J is the maximum number of iterations in Algorithm 2. In contrast, the SP algorithm exhibits a computational complexity of $\mathcal{O}(P_y L \log(K_s))$ in scenarios where \mathbf{h} is highly sparse. Therefore, while SBL achieves better performance, it does so at the cost

of higher computational complexity compared to the SP algorithm.

In RIS-assisted scenarios, however, the number of nonzero elements in the effective channel vector increases due to the presence of reflected paths. As a result, the channel becomes less sparse, and the complexity of the SP algorithm increases to $\mathcal{O}(P_y L K_s)$, since the previous complexity expression is only valid for highly sparse vectors.

4.3.2 A Low-Complexity Scheme with RIS Phase Optimization

The choice of reflection coefficients for the RIS elements is crucial to system performance. Each element's reflection coefficient is expressed as $\varphi_i e^{j\theta_i}$ for $i = 1, \dots, N_{\text{RIS}}$. For simplicity and without loss of generality, we assume $\varphi_i = 1$ for all elements so that only the phase θ_i is optimized. A key advantage of RIS is its ability to dynamically adjust these reflection coefficients in response to changing channel conditions. Since our channel is represented in the delay-Doppler domain—which exhibits slower variations than its time-frequency counterpart—the required frequency of phase adjustments is reduced compared to RIS systems employing OFDM. Expanding the effective channel in the delay-Doppler domain as in (32), the overall channel gain for the p th path ($p = 0, \dots, \check{P} - 1$) can be expressed as $h_{d,p} + \sum_{i=1}^{N_{\text{RIS}}} e^{j\theta_i} \mathfrak{h}_{i,p}$, where $h_{d,p}$ represents the direct channel gain and $\mathfrak{h}_{i,p}$ denotes the effective cascaded channel contribution from the i th RIS element (obtained from $\mathbf{B}^{(i)} \mathbf{G}^{(i)}$). Ideally, the RIS would adjust its phases to ensure that the reflected signals add constructively with the direct path, which would require

$$\angle h_{d,p} = \theta_i + \angle \mathfrak{h}_{i,p}, \quad \forall i = 1, \dots, N_{\text{RIS}} \text{ and } p = 0, \dots, \check{P} - 1. \quad (46)$$

In practice, however, a single phase shift per RIS element cannot simultaneously achieve coherent combining for all multipath components, particularly in multi-tap channels.

A more practical approach is to optimize the RIS phases to maximize the overall system capacity. The capacity for the RIS-assisted GFDM system is given by [58]

$$C = \frac{1}{MN} \log_2 \left| \mathbf{I}_{MN} + \frac{P_t \tilde{\mathbf{H}}_{\text{eff}}^H \tilde{\mathbf{H}}_{\text{eff}}}{MN \sigma^2} \right|, \quad (47)$$

where P_t is the transmit power. The corresponding optimization problem is formulated as

$$\begin{aligned} \max_{\Phi} \quad & \log_2 \left| \mathbf{I}_{MN} + \frac{P_t \tilde{\mathbf{H}}_{\text{eff}}^H \tilde{\mathbf{H}}_{\text{eff}}}{MN \sigma^2} \right|, \\ \text{s.t.} \quad & 0 \leq \theta_i < 2\pi, \quad i = 1, \dots, N_{\text{RIS}}. \end{aligned} \quad (48)$$

Solving (48) directly can be computationally intensive. To reduce complexity, we propose to align only the strongest delay-Doppler channel path. In our delay-Doppler-domain representation, the channel power is localized and sparse; thus, we select the dominant path \hat{p} that maximizes the effective channel gain:

$$\hat{p} = \arg \max_p \left[|h_{d,p}| + \sum_{i=1}^{N_{\text{RIS}}} |\mathbf{h}_{i,p}| \right]^2, \quad p \in \{0, \dots, \check{P} - 1\}. \quad (49)$$

Once the dominant path \hat{p} is identified, the RIS phase coefficients are tuned to align the reflected signals with the direct channel. Specifically, the optimal phase for each RIS element is given by

$$\hat{\theta}_i = \angle h_{d,\hat{p}} - \angle \mathbf{h}_{i,\hat{p}}, \quad i = 1, \dots, N_{\text{RIS}}. \quad (50)$$

This low-complexity approach effectively enhances the constructive combining of the reflected and direct signals, thereby maximizing the overall channel gain and system capacity.

4.4 Simulations

In this section, we present simulation results to evaluate the performance of our proposed channel estimation and RIS phase optimization methods for RIS-assisted GFDM systems. The simulation parameters are presented in Table 4.1. As shown in this table, the GFDM system employs 75 subcarriers and 75 subsymbols. The carrier frequency is set to 4 GHz, with a subcarrier spacing of 15 kHz. We use a synthetic Rayleigh channel model characterized by a maximum delay of 4 and a maximum Doppler shift of 3, corresponding to an approximate maximum Doppler speed of 160 km/h. An RC prototype filter with a roll-off factor of 0.5 is applied throughout.

Fig. 4.4 shows the MSE vs SNR performance of the proposed channel estimation method for

Table 4.1: Simulation Parameters for SBL-based algorithm

Parameter	Value	Description
M	75	Number of subsymbols
N	75	Number of subcarriers
f_c	4 GHz	Carrier frequency
Δf	15 kHz	Subcarrier spacing
l_{\max}	4	Maximum delay
k_{\max}	3	Maximum Doppler (Speed: 160 kmph)
α_r	0.5	Roll-off factor (raised cosine filter)

different numbers of pilot symbols. The results demonstrate that the SBL-based estimator outperforms the SP algorithm when fewer pilot symbols are used, owing to the fact that the measurement vector $\mathbf{y}_{p,dd}$ contains fewer elements than the number of non-zero components in the channel vector \mathbf{h} . Although the performance of the SP estimator improves with an increased number of pilot symbols, this comes at the expense of spectral efficiency.

Figure 4.5 presents the MSE performance as a function of the number of pilot symbols for the SBL-based approach. The proposed method achieves a lower MSE compared to standard approaches while remaining close to the Oracle-MMSE performance. As expected, increasing the number of pilot symbols improves estimation accuracy, with the gap between different estimators gradually reducing. The CRB remains the benchmark for unbiased estimators, while the Oracle-MMSE serves as the lower bound for biased approaches. Note that the difference in the starting point of the pilot number axis compared to Fig. 3.7 is due to the presence of the RIS in this scenario. The inclusion of three different channels in our simulation necessitates a larger guard interval, increasing the minimum required number of pilots compared to the previous chapter.

Fig. 4.6 illustrates the achievable rate for three scenarios: (i) with optimized RIS phase selection, (ii) with random RIS phase selection, and (iii) without RIS. In these simulations, the number of RIS elements is fixed at 100. The results show that the optimized RIS configuration—where the RIS phases are chosen based on the strongest delay-Doppler channel path—achieves the highest rate. In contrast, the system with random phase selection yields an intermediate performance, while the system without any RIS support attains the lowest achievable rate.

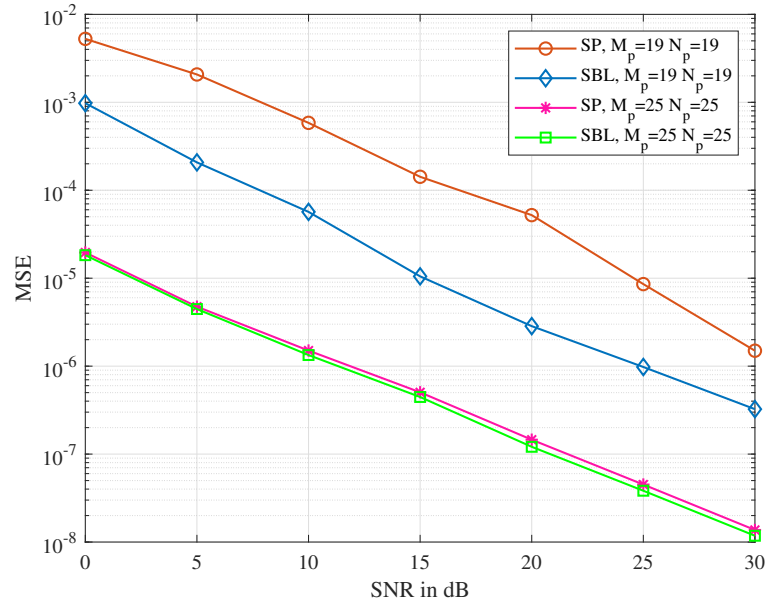


Figure 4.4: MSE performance comparison between the proposed SBL-based channel estimator and the SP algorithm at a Doppler speed of 160 km/h.

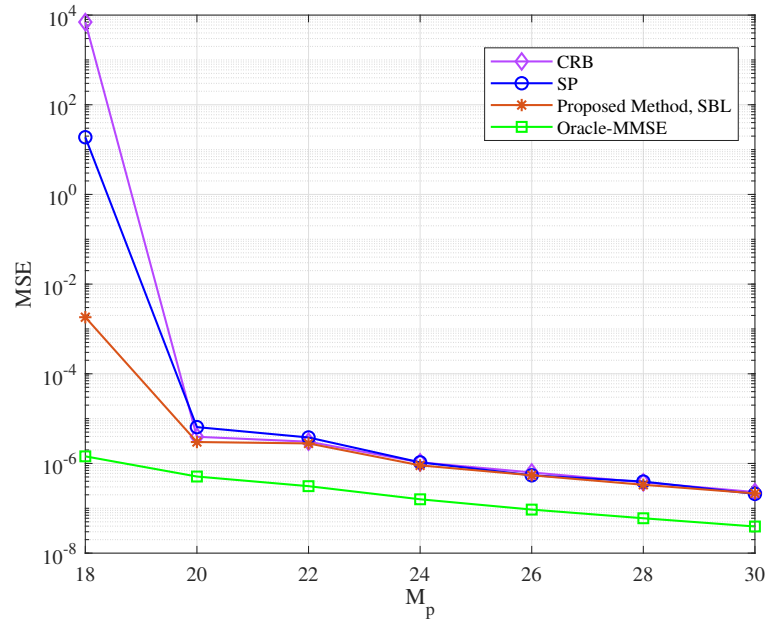


Figure 4.5: MSE performance comparison among the proposed SBL-based channel estimator, the SP algorithm, and the theoretical benchmarks (CRB and Oracle-MMSE) at an SNR of 10 dB, where $M_p = N_p$.

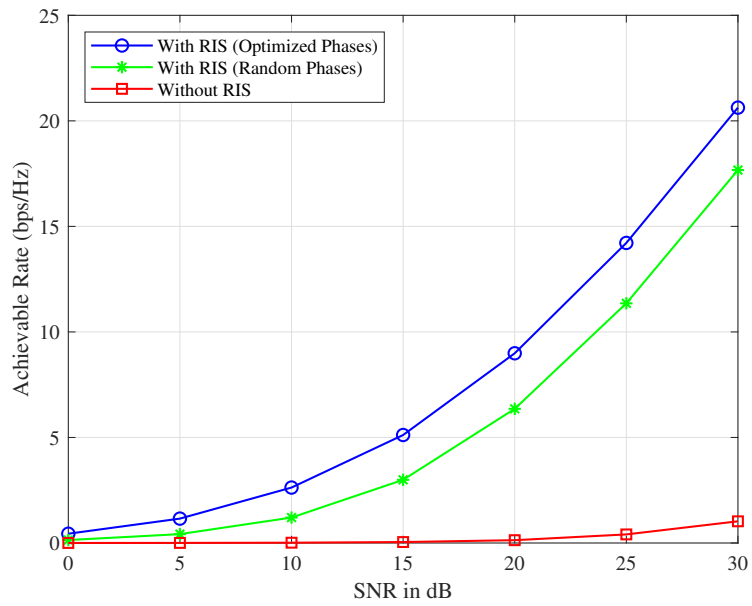


Figure 4.6: Achievable rate for three scenarios: optimized RIS phase selection, random RIS phase selection, and without RIS, with 100 RIS elements.

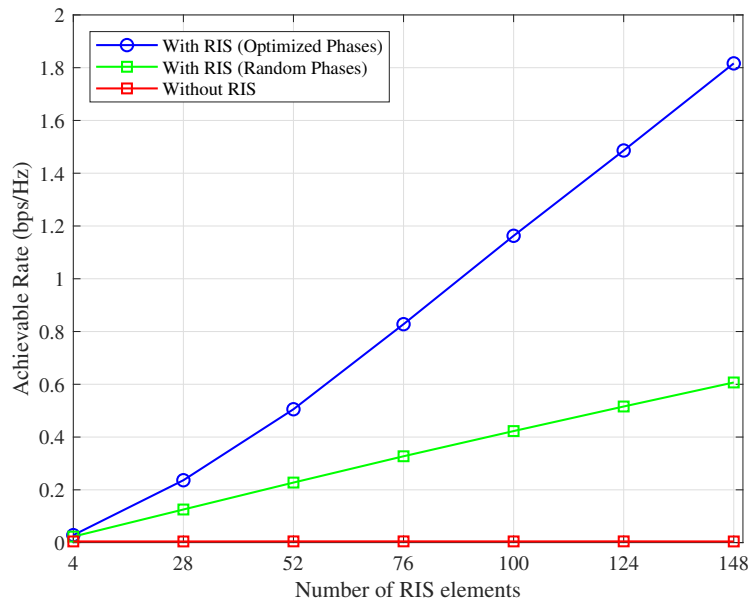


Figure 4.7: Achievable rate versus the number of RIS elements at an SNR of 10 dB.

Fig. 4.7 illustrates the achievable rate as a function of the number of RIS elements, at a fixed SNR of 10 dB. The results clearly indicate that the performance gain of the RIS-assisted GFDM system increases with the number of RIS elements, especially when the RIS phases are optimized as opposed to being randomly assigned. This confirms the effectiveness of our low-complexity RIS phase optimization strategy in enhancing the overall system capacity.

4.5 Conclusion

In this chapter, we presented a novel method for channel estimation in RIS-assisted GFDM systems based on SBL. By leveraging the inherent sparsity of the channel in the delay-Doppler domain, our approach utilizes the benefits of RIS to enhance system performance, notably in terms of achievable rate and reliability. The RIS provides an additional degree of freedom by enabling dynamic phase adjustments at its reflecting elements, which significantly improve the overall signal quality and capacity.

A key advantage of our SBL-based method is its robustness compared to conventional greedy algorithms, such as SP. Unlike SP, which requires a priori knowledge of the channel's sparsity level—a parameter that is difficult to determine in practice—the SBL framework inherently integrates this uncertainty into its probabilistic model. Furthermore, SBL is less sensitive to the choice of the sensing matrix, making it a more versatile and reliable tool for channel estimation in dynamic wireless environments.

Overall, the integration of RIS with GFDM, combined with the robust channel estimation capabilities of SBL, offers a promising solution for high-mobility communication scenarios. This approach not only enhances spectral efficiency and system capacity but also paves the way for more reliable data detection under challenging propagation conditions.

Chapter 5

Conclusion and Future Work

5.1 Conclusion

In this thesis, we have developed a comprehensive framework for enhancing channel estimation and overall system performance in high-mobility wireless communications by leveraging a novel representation of the GFDM system in the delay-Doppler domain. Traditional GFDM systems, typically designed in the time-frequency domain, often struggle with rapidly time-varying channels encountered in high-speed scenarios. To address this challenge, we proposed a new system model that transforms the GFDM signal into the delay-Doppler domain, where the channel exhibits a sparse structure. This representation not only simplifies the mathematical modeling of the channel but also enables more efficient signal processing techniques, particularly in the context of compressed sensing and sparse recovery. In our proposed model, both pilot and data symbols are superimposed in the delay-Doppler domain. This superimposed pilot scheme, which eliminates the need for dedicated pilot-only regions, leads to enhanced spectral efficiency without compromising the accuracy of channel estimation.

Based on the proposed system model, two channel estimation methods were investigated. In the first approach, we employed a compressed sensing technique using the Subspace Pursuit (SP) algorithm. This method exploits the sparsity of the channel by reconstructing the channel vector from a limited number of measurements and offers low computational complexity, which is advantageous for real-time applications. However, one limitation of the SP algorithm is its reliance on

prior knowledge of the sparsity level, which can be challenging to determine in practice.

To overcome the limitations of the SP algorithm, we developed a second method based on Sparse Bayesian Learning (SBL). Unlike conventional greedy algorithms, the SBL framework incorporates prior information about the channel's sparse structure directly into the Bayesian inference process. This probabilistic approach is inherently robust to the choice of sensing matrix and does not require a priori knowledge of the sparsity level, making it particularly well-suited for real-world applications where such information is not readily available. Simulation results confirmed that the SBL-based estimator achieved lower mean squared error (MSE) and superior performance compared to the SP algorithm, especially in scenarios with limited pilot overhead.

Building on the SBL framework, we further extended our system to include RIS panels. The incorporation of RIS into the GFDM system introduces additional degrees of freedom by enabling dynamic adjustment of the reflection coefficients. These coefficients are optimized to enhance the effective channel gain by aligning the reflected signals with the direct channel. Our RIS phase optimization strategy was designed to maximize the overall system capacity while maintaining low computational complexity. The optimization problem was formulated to maximize the achievable rate, and a low-complexity solution was derived by focusing on the dominant path in the delay-Doppler domain. The simulation results demonstrated that the RIS-assisted GFDM system, when combined with the SBL-based channel estimator, significantly outperformed conventional systems, both in terms of achievable rate and reliability.

The proposed methods were evaluated through extensive simulations. The results showed that our approach not only improves channel estimation accuracy and system capacity but also exhibits robustness under various mobility conditions and pilot configurations. In particular, the combination of the delay-Doppler domain representation, the superimposed pilot technique, and the SBL-based estimation provides a powerful tool for dealing with the challenges posed by high-mobility channels. Moreover, the integration of RIS further enhances the performance by enabling adaptive control over the propagation environment, leading to a more reliable and higher-capacity communication link.

5.2 Future Work

While the proposed framework has demonstrated promising improvements in channel estimation and RIS phase optimization for high-mobility GFDM systems, several research directions remain to be explored to further enhance performance and practicality.

One limitation of the current work is the assumption of integer Doppler shifts. In practical scenarios, the Doppler shift often contains a fractional component due to the limited resolution of the Doppler axis. Future work should extend the channel model to incorporate fractional Doppler shifts, which will likely require the development of advanced signal processing techniques to accurately resolve and compensate for these effects.

Another important direction is the extension of the current single-antenna framework to a multiple-input multiple-output (MIMO) configuration. MIMO systems can provide significant improvements in capacity and reliability by exploiting spatial diversity and multiplexing gains. Integrating MIMO techniques with the delay-Doppler domain representation and RIS-assisted communications could lead to substantial performance enhancements in high-mobility environments.

Reducing the computational complexity of the SBL algorithm is also a critical area for future research. The current SBL formulation requires the inversion of a matrix in every iteration, which can be computationally intensive. Investigating approximate inference methods or iterative techniques that bypass full matrix inversion could yield a more efficient algorithm without compromising estimation accuracy.

Furthermore, while our low-complexity RIS phase optimization strategy provides notable gains, exploring alternative optimization algorithms could further improve system performance. Advanced optimization techniques, such as deep learning-based approaches, may offer more precise phase alignment, thereby maximizing the effective channel gain and overall system capacity.

Finally, the extension of the proposed framework to multi-user scenarios represents a significant challenge and opportunity. In realistic wireless networks, multiple users share the communication resources, and inter-user interference becomes a critical factor. Future work should investigate multi-user scheduling, interference management, and resource allocation strategies within the context of RIS-assisted GFDM systems to enhance overall network scalability and performance.

Addressing these challenges will pave the way for more robust, efficient, and scalable wireless communication systems capable of operating under diverse and dynamic conditions. The insights gained from these future investigations are expected to further solidify the potential of delay-Doppler domain-based techniques, RIS-assisted communications, and advanced channel estimation algorithms in next-generation wireless networks.

References

- [1] I. F. Akyildiz, A. Kak and S. Nie, "6G and Beyond: The Future of Wireless Communications Systems," in *IEEE Access*, vol. 8, pp. 133995-134030, 2020.
- [2] A. Gupta and R. K. Jha, "A Survey of 5G Network: Architecture and Emerging Technologies," in *IEEE Access*, vol. 3, pp. 1206-1232, 2015.
- [3] T. Hwang, C. Yang, G. Wu, S. Li and G. Ye Li, "OFDM and Its Wireless Applications: A Survey," in *IEEE Transactions on Vehicular Technology*, vol. 58, no. 4, pp. 1673-1694, May 2009.
- [4] Y. Zhou et al., "Overview and Performance Analysis of Various Waveforms in High Mobility Scenarios," *2024 7th International Conference on Communication Engineering and Technology (ICCET)*, Tokyo, Japan, pp. 35-40, 2024.
- [5] B. Ai et al., "Challenges Toward Wireless Communications for High-Speed Railway," in *IEEE Transactions on Intelligent Transportation Systems*, vol. 15, no. 5, pp. 2143-2158, Oct. 2014.
- [6] N. Michailow *et al.*, "Generalized frequency division multiplexing for 5th generation cellular networks," *IEEE Transactions on Communications*, vol. 62, no. 9, pp. 3045-3061, Sept. 2014.
- [7] H. Shayanfar, H. Saeedi-Sourck and A. Farhang, "CFO and channel estimation techniques for GFDM," in *IEEE MTT-S International Microwave Workshop Series on 5G Hardware and System Technologies (IMWS-5G)*, 2018.

- [8] S. Ehsanfar, M. Matthé, M. Chafii and G. P. Fettweis, "Pilot- and CP-Aided Channel Estimation in MIMO Non-Orthogonal Multi-Carriers," in *IEEE Transactions on Wireless Communications*, vol. 18, no. 1, pp. 650-664, Jan. 2019.
- [9] A. Mohammadian and C. Tellambura, "Joint Channel and Phase Noise Estimation and Data Detection for GFDM," in *IEEE Open Journal of the Communications Society*, vol. 2, pp. 915-933, 2021.
- [10] A. M. Bello, W. Suwansantisuk, I. Song and T. Hirano, "Joint Synchronization and Channel Estimation for GFDM Systems," in *IEEE Access*, vol. 12, pp. 138061-138075, 2024.
- [11] S. Ehsanfar, M. Chafii and G. Fettweis, "Time-variant pilot- and CP- aided channel estimation for GFDM," in *IEEE International Conference on Communications (ICC)*, pp. 1-6, 2019.
- [12] Tian, X., Liu, C., Gu, Y. et al. "Channel estimation of GFDM system based on pilot frequency in doubly selective channel". *Wireless Netw* 30, 5049–5057 (2024).
- [13] R. Hadani *et al.*, "Orthogonal time frequency space modulation," in *Proc. IEEE Wireless Commun. Netw. Conf.*, pp. 1–6, Mar. 2017.
- [14] L. Xiao, S. Li, Y. Qian, D. Chen and T. Jiang, "An Overview of OTFS for Internet of Things: Concepts, Benefits, and Challenges," in *IEEE Internet of Things Journal*, vol. 9, no. 10, pp. 7596-7618, 15 May 15, 2022.
- [15] P. Raviteja, K. T. Phan and Y. Hong, "Embedded Pilot-Aided Channel Estimation for OTFS in Delay–Doppler Channels," in *IEEE Transactions on Vehicular Technology*, vol. 68, no. 5, pp. 4906-4917, May 2019.
- [16] W. Shen, L. Dai, J. An, P. Fan and R. W. Heath, "Channel Estimation for Orthogonal Time Frequency Space (OTFS) Massive MIMO," in *IEEE Transactions on Signal Processing*, vol. 67, no. 16, pp. 4204-4217, 15 Aug. 15, 2019.
- [17] Y. Zhang, Q. Zhang, C. He, L. Jing, T. Zheng and C. Yuen, "Sparse Bayesian Learning Approach for OTFS Channel Estimation With Fractional Doppler," in *IEEE Transactions on Vehicular Technology*, vol. 73, no. 11, pp. 16846-16860, Nov. 2024.

- [18] P. Raviteja, Y. Hong, E. Viterbo and E. Biglieri, "Practical pulse-shaping waveforms for reduced-cyclic-prefix OTFS," *IEEE Transactions on Vehicular Technology*, vol. 68, no. 1, pp. 957-961, Jan. 2019.
- [19] S. Kalsotra, A. Kumar, H. D. Joshi, A. K. Singh, K. Dev and M. Magarini, "Impact of Pulse Shaping Design on OOB Emission and Error Probability of GFDM," 2019 IEEE 2nd 5G World Forum (5GWF), Dresden, Germany, pp. 226-231, 2019.
- [20] A. Nimr, M. Chafii, M. Matthe and G. Fettweis, "Extended GFDM framework: OTFS and GFDM comparison," in *IEEE Global Communications Conference (GLOBECOM)*, pp. 1-6, 2018.
- [21] B. Zheng, C. You, W. Mei and R. Zhang, "A Survey on Channel Estimation and Practical Passive Beamforming Design for Intelligent Reflecting Surface Aided Wireless Communications," in *IEEE Communications Surveys Tutorials*, February 2022.
- [22] A. Taha, M. Alrabeiah and A. Alkhateeb, "Enabling Large Intelligent Surfaces With Compressive Sensing and Deep Learning," in *IEEE Access*, vol. 9, pp. 44304-44321, 2021.
- [23] Y. Yang, B. Zheng, S. Zhang and R. Zhang, "Intelligent Reflecting Surface Meets OFDM: Protocol Design and Rate Maximization," in *IEEE Transactions on Communications*, vol. 68, no. 7, pp. 4522-4535, July 2020.
- [24] B. Zheng and R. Zhang, "Intelligent Reflecting Surface-Enhanced OFDM: Channel Estimation and Reflection Optimization," in *IEEE Wireless Communications Letters*, vol. 9, no. 4, pp. 518-522, April 2020.
- [25] B. Zheng, C. You and R. Zhang, "Fast Channel Estimation for IRS-Assisted OFDM," in *IEEE Wireless Communications Letters*, vol. 10, no. 3, pp. 580-584, March 2021.
- [26] A. Taha, M. Alrabeiah and A. Alkhateeb, "Enabling Large Intelligent Surfaces With Compressive Sensing and Deep Learning," in *IEEE Access*, vol. 9, pp. 44304-44321, 2021.

- [27] S. M. J. A. Tabatabaee, M. Towliat, M. Rajabzadeh and F. S. Khodadad, "Intelligent-Reflecting-Surface-Assisted GFDM Communication Systems," in *IEEE Systems Journal*, vol. 17, no. 2, pp. 2858-2867, June 2023.
- [28] H. Shayanfar, W. P. Zhu and M. N. S. Swamy, "Compressed Sensing Based Channel Estimation for GFDM Systems in High Mobility Scenario," *IEEE 24th International Workshop on Signal Processing Advances in Wireless Communications (SPAWC)*, Shanghai, China, 2023.
- [29] H. Shayanfar, W. P. Zhu and M. N. S. Swamy, "Sparse Bayesian Learning Channel Estimation and Phase Optimization for RIS-Assisted GFDM System" *submitted to the IEEE Vehicular Technology Conference (VTC2025-Fall)*, Chengdu, China, 2025..
- [30] Z. Wei et al., "Orthogonal Time-Frequency Space Modulation: A Promising Next-Generation Waveform," in *IEEE Wireless Communications*, vol. 28, no. 4, pp. 136-144, August 2021.
- [31] Y. Hong, T. Thaj and E. Viterbo, *Delay-Doppler Communications: Principles and Applications*, Academic Press, Elsevier, 2022.
- [32] I. S. Gaspar, L. L. Mendes, N. Michailow, and G. Fettweis "A synchronization technique for generalized frequency division multiplexing," *EURASIP J. Adv. Signal Process.*, vol. 2014, no. 1, p. 67, Dec. 2014.
- [33] I. S. Gaspar, *Waveform Advancements and Synchronization Techniques for Generalized Frequency Division Multiplexing*, Technische University Dresden, 2016.
- [34] N. Michailow, S. Krone, M. Lentmaier and G. Fettweis, "Bit Error Rate Performance of Generalized Frequency Division Multiplexing," *2012 IEEE Vehicular Technology Conference (VTC Fall)*, Quebec City, QC, Canada, 2012.
- [35] H. Shayanfar, H. Saeedi-Sourck, A. Farhang, and L. E. Doyle, "Maximum-likelihood synchronization and channel estimation with multiuser detection in GFDMA," *Trans. Emerg. Telecommun. Technol.*, vol. 29, no. 6, p. e3424, Jun. 2018.

- [36] A. Farhang, N. Marchetti and L. E. Doyle, "Low complexity GFDM receiver design: A new approach," *2015 IEEE International Conference on Communications (ICC)*, London, UK, 2015.
- [37] P. Raviteja et al., "Interference cancellation and iterative detection for orthogonal time frequency space modulation," *IEEE Trans. Wireless Commun.*, vol. 17, no. 10, pp. 6501–6515, Oct. 2018.
- [38] C. E. Shannon, "Communication in the presence of noise," *Proc. Inst. Radio Eng.*, vol. 37, no. 1, pp. 10–21, Jan. 1949.
- [39] E. Crespo Marques, N. Maciel, L. Naviner, H. Cai and J. Yang, "A review of sparse recovery algorithms," in *IEEE Access*, vol. 7, pp. 1300-1322, 2019.
- [40] . J. Mechery, M. Remadevi, "Compressive sensing based underwater channel estimation", *Elsevier Journal*, V. 115, P. 683-690, 2017.
- [41] Y. C. Pati, R. Rezaifar, and P. S. Krishnaprasad, "Orthogonal matching pursuit: recursive function approximation with applications to wavelet decomposition," in *Proceedings of 27th Asilomar Conference on Signals, Systems and Computers*, pp. 40–44 vol.1, Nov, 1993.
- [42] W. Dai and O. Milenkovic, "Subspace pursuit for compressive sensing signal reconstruction," *IEEE Transactions on Information Theory*, vol. 55, no. 5, pp. 2230- 2249, May 2009.
- [43] J. Tropp, D. Needell, and R. Vershynin, "Iterative signal recovery from incomplete and inaccurate measurements," in *Proc. Information Theory and Applications Workshop*, San Deigo, CA, Feb. 2008.
- [44] E. Candès, J. Romberg, and T. Tao, "Robust uncertainty principles: exact signal reconstruction from highly incomplete frequency information," *IEEE Trans. Inf. Theory*, vol. 52, no. 2, pp. 489–509, Feb. 2006.
- [45] I. E. Nesterov, A. Nemirovskii, and Y. Nesterov, *Interior-Point Polynomial Algorithms in Convex Programming*. Philadelphia, PA: SIAM, 1994.

- [46] W. D. Dias, L. L. Mendes and J. J. P. C. Rodrigues, "Low complexity GFDM receiver for frequency-selective channels," *IEEE Communications Letters*, vol. 23, no. 7, pp. 1166-1169, July 2019.
- [47] M. Ghogho, D. McLernon, E. Alameda-Hernandez and A. Swami, "Channel estimation and symbol detection for block transmission using data-dependent superimposed training," *IEEE Signal Processing Letters*, vol. 512, no. 3, pp. 226-229, March 2005.
- [48] S. M. Kay, *Fundamentals of Statistical Signal Processing: Estimation Theory*, Englewood Cliffs, NJ, USA:Prentice-Hall, vol. 1, 1998.
- [49] Y. C. Eldar and G. Kutyniok, *Compressed Sensing: Theory and Applications*, Cambridge, U.K:Cambridge Univ. Press, 2012.
- [50] S. Srivastava, R. K. Singh, A. K. Jagannatham and L. Hanzo, "Bayesian Learning Aided Sparse Channel Estimation for Orthogonal Time Frequency Space Modulated Systems," *IEEE Transactions on Vehicular Technology*, vol. 70, no. 8, pp. 8343-8348, Aug. 2021.
- [51] Q. Wu, S. Zhang, B. Zheng, C. You and R. Zhang, "Intelligent Reflecting Surface-Aided Wireless Communications: A Tutorial," in *IEEE Transactions on Communications*, vol. 69, no. 5, pp. 3313-3351, May 2021.
- [52] Z. Wei, W. Yuan, S. Li, J. Yuan and D. W. K. Ng, "Off-Grid Channel Estimation With Sparse Bayesian Learning for OTFS Systems," in *IEEE Transactions on Wireless Communications*, vol. 21, no. 9, pp. 7407-7426, Sept. 2022.
- [53] S. D. Babacan, R. Molina, and A. K. Katsaggelos, "Bayesian compressive sensing using laplace priors," *IEEE Trans. Image Process.*, vol. 19, no. 1, pp. 53–63, Jan. 2010.
- [54] M. E. Tipping, "Sparse Bayesian learning and the relevance vector machine," *J. Mach. Learn. Res.*, vol. 1, pp. 211–244, Sep. 2001.
- [55] Z. Yang, L. Xie, and C. Zhang, "Off-grid direction of arrival estimation using sparse Bayesian inference," *IEEE Trans. Signal Process.*, vol. 61, no. 1, pp. 38–43, Jan. 2013.

- [56] K. You, W. Guo, Y. Liu, W. Wang and Z. Sun, "Grid Evolution: Joint Dictionary Learning and Sparse Bayesian Recovery for Multiple Off-Grid Targets Localization," in *IEEE Communications Letters*, vol. 22, no. 10, pp. 2068-2071, Oct. 2018.
- [57] M. E. Tipping, "Sparse Bayesian learning and the relevance vector machine," *J. Mach. Learn. Res.*, vol. 1, pp. 211–244, Sep. 2001.
- [58] S. K. Mohammed, "Time-domain to delay-Doppler domain conversion of OTFS signals in very high mobility scenarios," *IEEE Trans. Veh. Technol.*, vol. 70, no. 6, pp. 6178–6183, Jun. 2021.